Superconducting nanostructures fabricated with the scanning tunnelling microscope

2004 J. Phys.: Condens. Matter 16 R1151

(http://iopscience.iop.org/0953-8984/16/34/R01)

INSTITUTE OF PHYSICS PUBLISHING JOURNAL OF PHYSICS: CONDENSED MATTER

J. Phys.: Condens. Matter **16** (2004) R1151–R1182 PII: S0953-8984(04)34230-X

TOPICAL REVIEW

Superconducting nanostructures fabricated with the scanning tunnelling microscope

J G Rodrigo[1], H Suderow[1], S Vieira[1,4], E Bascones[2] and F Guinea[3]

[1] Laboratorio de Bajas Temperaturas, Departamento de Física de la Materia Condensada, Instituto de Ciencia de Materiales Nicolás Cabrera, Universidad Autónoma de Madrid, 28049 Madrid, Spain
[2] Theoretische Physik, ETH-Hönggerberg, CH-8093 Zürich, Switzerland
[3] Instituto de Ciencia de Materiales de Madrid, CSIC, Cantoblanco, 28049 Madrid, Spain

E-mail: sebastian.vieira@uam.es

Received 26 May 2004
Published 13 August 2004
Online at stacks.iop.org/JPhysCM/16/R1151
doi:10.1088/0953-8984/16/34/R01

Abstract

The properties of nanoscopic superconducting structures fabricated with a scanning tunnelling microscope are reviewed, with emphasis on the effects of high magnetic fields. These systems include the smallest superconducting junctions which can be fabricated, and they are a unique laboratory in which to study superconductivity under extreme conditions. The review covers a variety of recent experimental results on these systems, highlighting their unusual transport properties, and theoretical models developed for their understanding.

Contents

[4] Author to whom any correspondence should be addressed.

1. Introduction

Soon after the transcendental discovery by Meissner in 1933 of perfect diamagnetism, as one of the characteristic features of the superconducting state [1], the London brothers published in 1935 an article entitled 'the electromagnetic equations of the superconductor' [2]. This article contains the well known London theory, which provided the first important approach to our macroscopic understanding of this phenomenon. Very soon one of the brothers, Heinz London, concluded from the theory that 'a very small superconductor should have a much higher magnetic threshold value than a bulky one' [3]. Pontius confirmed this prediction experimentally two years later [4, 5]. In 1939 Appleyard *et al* [6] found an increase of the magnetic threshold to more than 20 times the bulk critical field in mercury films as thin as 57 nm. Shoenberg [7] observed this effect by measuring the magnetic susceptibility of very fine-grained preparations of colloidal mercury in 1940. From then to now, there have been many important developments both in theory and experiment, including several milestones such as the Ginzburg–Landau (GL) theory [8], the microscopic BCS theory [9], the Josephson effects [10], the type II superconductors [11] and the discovery of high-T_c superconducting oxides [12]. GL theory has proven itself as a very important tool which separates superconductors into two types (I and II), depending on their response to external magnetic fields. Abrikosov predicted [11] the real existence of type II superconductors, with the characteristic mixed or vortex state present in a wide range of magnetic fields. Tinkham [13] pointed out that sufficiently thin films of any material should exist in the mixed state even if thicker specimens of the same material exhibit a type I behaviour. This vortex state was visualized later on in magnetic decoration experiments [14, 15].

Today superconductivity is one of the most flourishing fields of condensed matter physics, showing many new interesting developments. A recent one is the reduction of the dimensions of the superconducting samples towards controlled three-dimensional mesoscopic structures. Electron lithography allows us to pattern different types of superconducting structures with all their dimensions of the same order as or smaller than the magnetic penetration depth of the bulk material [16–18]. Many experimental and theoretical [19, 20] developments on mesoscopic superconductivity have been made, unravelling new physics related to the confinement of the condensate. Experiments with single small particles [21], thin wires [22, 23], carbon nanotubes [24, 25] or DNA molecules [26–28] have been reported. Very clever solutions have been given to the difficult problem of the contacts (see e.g. [27]), although it remains one of the main limitations in the operation of these small systems [29, 30].

The invention of the scanning tunnelling microscope [31], STM, has been a breakthrough towards our control of the nanoworld. Following this invention, several tools have been developed extending the initial STM capabilities. Atomic force microscopy [32] has proven to be a powerful tool to investigate both fundamental problems and others with particular technological importance, such as friction, wear or fracture. Imaginative combinations of the working principles of both techniques have promoted new tools for specific experiments. Among them, we highlight the results by Rubio-Bollinger *et al* [33], that were able to measure force and conductance simultaneously, extracting one atom after another from a surface, and creating the smallest and thinnest arrangement of atoms ever made, an atomic chain. Magnetic force microscopy [34] and scanning Hall probe microscopy [35] are other useful members of this toolkit, whose main achievements rest on the impressive control of the displacements that can be done through the piezoelectric deformation of some ceramic materials. This control is magnified at low temperatures where atomic mobility is very low and the creep effect in the piezoelectric ceramics is also reduced to a very low level [36]. There are many relevant achievements in condensed matter physics that have appeared in the 20 year span since the

STM invention. One of these, related to the main topic of this review, was the observation of an atomic jump to contact when a metallic atomically sharp tip was carefully approached to a sample of the same material [37]. Since this pioneering experiment many others have been done to study transport and mechanical properties of atomic-size contacts using an STM [38]. Taking advantage of the unprecedented capability of control that STM has on the displacements, nanometric indentations of the tip in the sample surface can be made to create bridges of variable minimal cross-section [39–42].

We will review here charge transport through superconducting nanobridges and related structures, and the physical information contained on this transport. The transport regime can be dramatically modified by small changes in the minimal cross-section region, the neck, but the overall nanostructure (nanobridge) remains unmodified when scanning through these regimes in the experiment. At a high level of current, heating and other nonequilibrium effects appear. In atomic-size contacts superconductivity and quantum transport phenomena can be studied in a well controlled manner. Breaking the tip into two parts results into two atomic size nanotips. One of these can be *in situ* transported elsewhere and used to perform atomic resolution microscopy and spectroscopy over a sample, without change in vacuum or temperature conditions [43]. The application of an external magnetic field confines the condensate around the bridge region, creating a nanoscopic superconductor with a perfect interface with the normal region, solving in a natural way the contacting problems [29] associated with this kind of structures. This unique system gives us the possibility to perform experiments in a highly controlled situation. Theoretical calculations using Ginzburg–Landau theory and Usadel equations provide a framework to understand the most important aspects of superconductivity in these bridges.

We discuss first how the nanostructures are built and characterized (section 2). Then, in section 3, we will review theoretical models and experimental results about the transport properties of these systems at zero magnetic field. We discuss separately the three different conduction regimes: tunnel, atomic contact and low-resistance ballistic transport. The same scheme is used to discuss the transport properties in an applied field (section 4). We conclude, in section 5, with comments on open questions and future studies which can be addressed with the systems described here.

2. Fabrication and characterization of the superconducting nanostructures

The scanning tunnelling (STM) [31] and the atomic force (AFM) [32] microscopes, as well as some related techniques, are versatile tools to penetrate the nanoworld realm. The STM allows us to study the topography and electronic properties of a conducting surface with atomic spatial resolution. In the little more than 20 years elapsed since its invention this technique has became widely used. These instruments can be obtained from commercial suppliers, some of them designed to work at low temperatures. However, home made STMs are in use in many laboratories, as they give the required versatility and accuracy for doing specific research. Some home made STMs are well adapted to be mounted in the cryogenic ambiance of ^{3}He–^{4}He dilution and ^{3}He refrigerators, and to work under magnetic fields [44–48]. A cylindrically symmetric design is best suited for that. In figure 1(a) we show a sketch of the STM built and used in the low-temperature laboratory of the Universidad Autonoma de Madrid [49], and highlight its original aspects. The coarse approach system, a piston whose controlled movement is produced by piezoelectric stacks, is designed to give, if wanted, strong indentation of the tip in the sample surface. With this system, tip and sample can be approached from distances of several millimetres *in situ* at low temperatures. A piezotube with capabilities of vertical displacements, at cryogenic temperatures, in the range of several tenths of microns

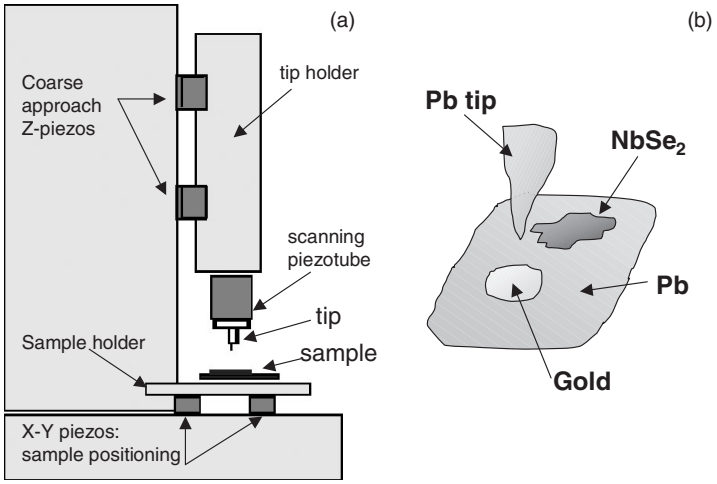

Figure 1. Scheme of the STM unit (a) and its composite sample holder (b) used in the low-temperature laboratory of the Universidad Autonoma de Madrid.

is used for the fine control and movement. The table on which the sample holder is located is the other important part of this instrument [49]. At low temperatures it can be moved in the x–y plane distances in the millimetric range using piezoelectric stacks. This movement is well controlled and reproducible, and allows us to access with the tip a wide surface area within the same cooling down run. Therefore, the sample holder can include a composite sample of different materials, which can be studied together (see figure 1(b)).

The structures that we discuss in this review have been obtained using superconducting materials and the STM as a tool for its fabrication. We call them nanobridges, because the dimensions of the largest ones are a few hundreds of nanometres. The fabrication of large nanobridges works well with ductile metals like Au, Pb, Al and Sn [38, 41, 50, 51] and semimetals, as is the case of Bi [52]. The first step of the fabrication is to crash, in a controlled manner, a clean tip into a clean substrate, normally both of the same material (see a schematic representation of the process in figure 2). As the tip is pressed against the substrate, both electrodes deform plastically and then bind by cohesive forces, forming a connective neck (figure 2(b)). Retraction of the tip results in the formation of the neck, that elongates plastically (figure 2, frames (c)–(e)) and eventually breaks (frame (f)).

Measuring the current, I, flowing through the neck at a fixed bias, usually between 10 and 100 mV, as a function of the displacement, z, of the tip relative to the substrate, it is possible to follow the evolution of the neck. These I–z curves are staircase-like and strikingly reproducible when the process is repeated many times [39, 51]. The detailed analysis of the last steps from these experiments, close to the breaking point of the nanobridge, is often represented as conductance histograms [38]. From those it has been possible to extract, for some simple metals, relevant information on quantum transport through atomic-size contacts.

It was soon understood that the staircase shape of the I–z curves reflected the sequence of elastic and plastic deformations followed by the nanobridge [53, 54]. Only the minimal cross section, which determines the conductance and the current I at a fixed voltage, is modified. This is a natural result, as the stress is mostly concentrated around the narrowest part of the nanobridge, the neck. The conclusive evidence came from the combined STM–AFM experiments [41, 50, 55], in which the conductance and the forces which develop

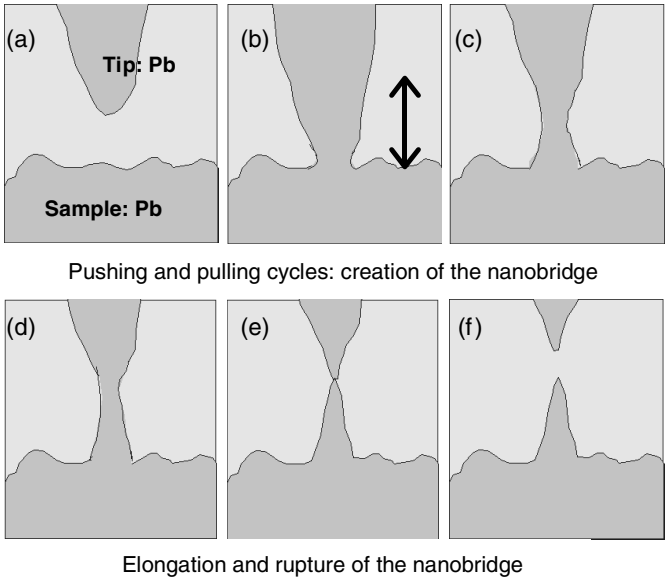

Figure 2. Sketch of the nanobridge fabrication process. Frames (a)–(f) illustrate different stages of the process: (a) tip and sample in tunnelling regime; (b) the tip is pressed against the substrate, both electrodes deform plastically and form a connective neck; (c)–(e) indentation–retraction cycles produce a plastic elongation of the neck; (f) the rupture of the nanobridge takes place.

during the elongation or contraction of the nanobridge were simultaneously measured. The intimate relation between conductance steps and atomic rearrangements was then established definitively. These experiments were performed with lead and gold, the noble metal being the material most thoroughly studied. It was even possible to observe how, during the elongation of the bridge, gold deforms plastically down to the last atom contact, and chains consisting of several atoms were created [33, 56].

The conductance observed for these gold atomic contacts is quite close to $1G_0$, where $G_0 = 2e^2/h$ is the value of the quantum of conductance [57, 58]. The force involved in the rupture of these one-atom contacts is also well defined, with a value of 1.5 ± 0.1 nN [33, 55]. Transport experiments in several other elements in the superconducting state (Pb, Al or Nb, and also in Au, made superconducting using the proximity effect), have permitted us to establish a clear relationship between the conductance of the last contact and the chemical nature of the atom involved [59–61]. Along with these experimental achievements there have been important and successful efforts to get a theoretical understanding of this subject. A recent review by Agraït *et al* [38] provides a comprehensive vision of this field.

Here we are mainly concerned with the overall shape of the nanobridges created with the STM and, in particular, using superconducting materials. The results shown in figure 3 were the first clear indication that the controlled fabrication of superconducting nanobridges using an STM as a tool and as a probe was possible [39]. In this experiment, performed at 4.2 K, high-purity lead ($T_c = 7.14$ K) was used for tip and sample. The current for a bias of 50 mV was measured, changing the area of the contact. Both quantities, minimal cross section and current, can be related using the simple Sharvin formula [62]:

$$G_S = \frac{2e^2}{h}\frac{k_F a}{2}^2 \tag{1}$$

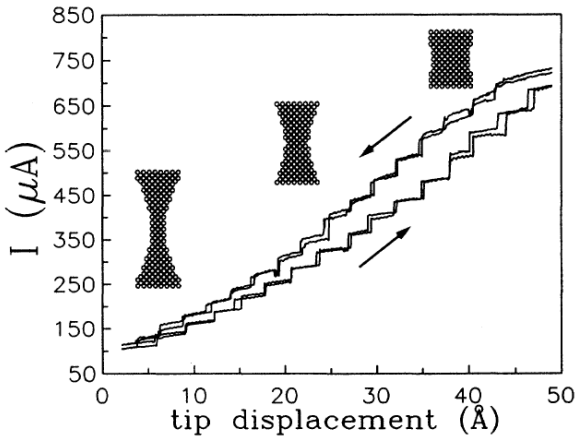

Figure 3. Experiments performed at 4.2 K, using a Pb tip and sample, from [39]. The current for a bias of 50 mV was measured, changing the area of the contact. A reproducible and regular structure in the current versus tip displacement curves develops. Remarkably, this high reproducibility is obtained in a process involving plastic deformations. The estimated shapes at different stages of the nanobridge along the I–z curves are sketched.

where $G_S = dI/dV$ is the conductance, a is the radius of the contact, k_F is the Fermi wavevector, h is Planck's constant and e is the electron charge. This expression is strictly valid for ballistic transport (i.e., electronic mean free path $\ell \gg a$) [38]. Assuming that deformations are confined to a small region of volume around the narrowest cross section, and that the neck is parabolic, the evolution of its shape can be obtained from the measured I–z curves (figure 3). Large nanobridges could be obtained with the procedure schematically represented in figure 4(a). Following a strong indentation the tip is receded while moving back and forth with a smaller amplitude without breaking the contact. Then a reproducible and regular structure in the current versus tip displacement curves develops.

Untiedt *et al* [51] developed a slab model suggested by the results of combined STM–AFM experiments. When the conductance is fairly constant, the force varies linearly, while the abrupt jumps in conductance are correlated to abrupt force relaxations. Between the relaxations deformation is elastic so that no energy is dissipated. The nanobridge is modelled as a constriction with cylindrical geometry, consisting of slabs of different radii and thickness, symmetrical with respect to its minimal cross section. The elastic properties of the nanobridge, e.g., Young's modulus E and Poisson's ratio μ, are considered identical to the bulk values. The basic assumption for this model is that only the narrowest part of the nanobridge, the neck, deforms plastically. This assumption could break down for temperatures larger than about 50% of the melting temperature, for which diffusion will be important [51, 63], but it is valid at the temperatures of interest for this review, where atomic mobility is negligible. The slab model provides a good description of the shape and dimensions of the scanned feature, left onto the surface of the sample after breaking a fabricated nanobridge. The atomic sharpness of the tips obtained using this method, permits us to obtain images with atomic resolution [43]. A composite sample like the one shown in figure 1(b) was used. After preparing an atomically sharp Pb tip on the lead surface, the sample holder is moved so that the $NbSe_2$ single-crystal surface could be reached and scanned by the tip.

Large-amplitude phonon peaks were observed in point contact spectroscopy experiments in long nanobridges with I–z curves showing prominent and repetitive stepped structure [51].

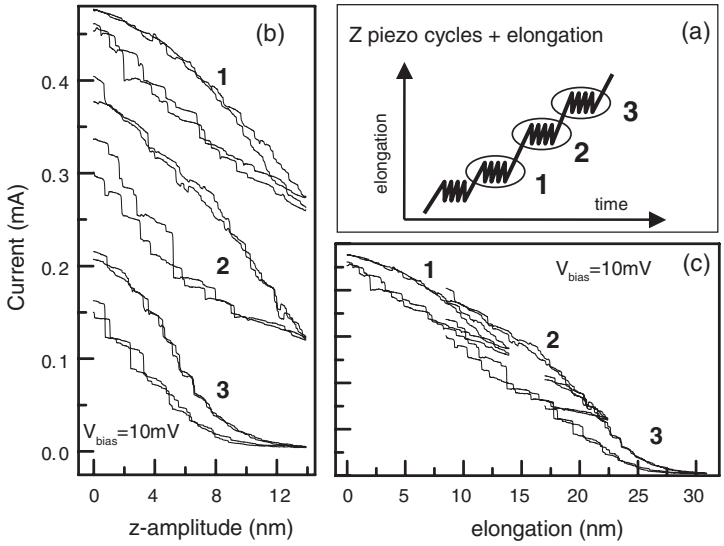

Figure 4. (a) Schematic indication of the time evolution of the process of elongation of the nanobridge. (b) I–z curves as recorded in a real nanobridge fabrication. Each group of curves (1, 2 and 3) corresponds to a different stage of the elongation of the nanobridge, i.e., a different neck. These curves can be arranged in order to account for the total elongation of the nanobridge (c). (Data from [64].)

This observation was interpreted as an indication of crystallinity due to 'mechanical annealing' of the defects by repeated plastic deformation.

3. Transport regimes in superconducting nanostructures at zero magnetic field

3.1. Theory

The current flowing through a tunnel junction (see [65] for a general review on tunnelling spectroscopy) is given by the convolution of the density of states (DOS) of both electrodes:

$$I = \frac{G_N}{e} \int_{-\infty}^{\infty} N_1(E) N_2(E) [f(E) - f(E + eV)] \, dE \tag{2}$$

where N_1 and N_2 are the normalized densities of states and G_N is the normal-state conductance of the junction.

For BCS superconducting electrodes, the density of states takes the form [9] $N(E) = \mathrm{Re}[E/\sqrt{E^2 - \Delta^2}]$, Δ being the superconducting gap. If tunnelling is performed between two identical superconductors, at zero temperature no current can flow for voltages $V < 2\Delta/e$. At finite temperatures, due to thermal excitations, states above the Fermi level can be populated and those below depopulated, allowing finite quasiparticle current flow at voltages smaller than $2\Delta/e$.

In tunnel junctions where the barrier is sufficiently low, multiple scattering of Cooper pairs leads to a finite conductance below the superconducting gap. In these processes, generically called Andreev reflection [66], an electron is reflected as a hole at the junction, leading to the transmission of a Cooper pair [67–71]. Subgap Andreev reflection takes place both in normal–superconductor junctions and in superconductor–superconductor junctions. A quantitative analysis of these processes in normal–superconductor (N–S) junctions was performed in [72],

and later extended to superconductor–superconductor junctions [73], where the junction was described as two superconductor–normal junctions in series. A complete determination of the transport properties of a superconductor–superconductor junction at finite voltages requires us to take into account not only the dc current, but also the higher harmonics. A detailed analysis of the time dependent current flowing under an arbitrary applied voltage, taking into account all multiple Andreev reflections (MAR), for a single channel through the junction, was done in [74] and in [75]. At large voltages $V \gg 2\Delta/e$, I–V curves are linear, with a slope given by the normal state conductance, but do not extrapolate to zero. The excess current [76] is defined by

$$I_{\mathrm{exc}} = \lim_{V\to\infty} [I(V) - I_{\mathrm{n}}(V)] \tag{3}$$

with I_{n} the current in the normal state. At low voltages $V \leqslant 2\Delta/e$, the I–V curves are strongly non-linear, showing inflections at $eV = 2\Delta/n$. These features, known as subharmonic gap structure (SGS), are a consequence of the multiple Andreev reflections. They can be modified by the internal structure of the junction, or when the transmission coefficient has a significant energy dependence [77].

The non-linearity of the I–V curves has been used to discuss the contribution from different channels in junctions of atomic dimensions [59, 60]. The current in a superconducting–superconducting constriction can be written as the sum of the contribution of N channels in parallel $I = \sum_{n=1}^{N} \mathrm{i}(V, T_{\mathrm{n}})$ [78]. The current carried by each channel is that corresponding to a one-dimensional superconducting constriction with transmission T_{n}. In the normal state, the total current depends only on the total conductance, independently of the transmission of the individual channels which contribute to it. This is not the case in the superconducting state. In an mth Andreev reflection process the barrier is transversed $m + 1$ times. The probability that this process occurs scales as T_{n}^{m+1}. Hence, the total current I strongly depends on the set of individual transmission coefficients.

The current through a superconductor–superconductor (S–S) junction shows other features due to the phase rigidity of the condensate. The most striking manifestation of this property is the Josephson effect [10, 79, 80]. A current below a certain value, I_{c}, can flow between two superconductors at zero voltage. Following Ambegaokar and Baratoff [81], the critical current, I_{c}, of a tunnel junction between BCS superconductors can be written as $I_{\mathrm{c}} \approx (\pi G_{\mathrm{N}}\Delta)/(2e)$. This analysis was later extended to other types of junctions [82]. The value of the critical current I_{c} for a short and narrow constriction was calculated by Kulik and Omel'yanchuk [83] in the case of a point contact much wider than the Fermi wavelength, when the quantization of the momentum can be neglected. Its value for a quantum point contact with a small number of conducting channels was calculated by Beenakker and van Houten [84, 85]. The observation of Josephson current is affected by the balance between the thermal energy, $k_{\mathrm{B}}T$, and the Josephson coupling energy [81], given by

$$E_{\mathrm{J}} = \frac{\Delta R_{\mathrm{Q}}}{2R_{\mathrm{N}}} \tag{4}$$

where R_{N} is the normal-state resistance and $R_{\mathrm{Q}} = h/4e^2 = 6.45\ \mathrm{k}\Omega$. For resistances such that the Josephson coupling energy is comparable to the thermal energy, the superconducting phase dynamics is dominated by thermal fluctuations, making the Josephson current appear as a peak centred at small finite voltage. In this case the phase motion can be viewed as diffusive. The I–V characteristics of such a junction have been calculated by several authors [86–90] using the washboard potential model [91].

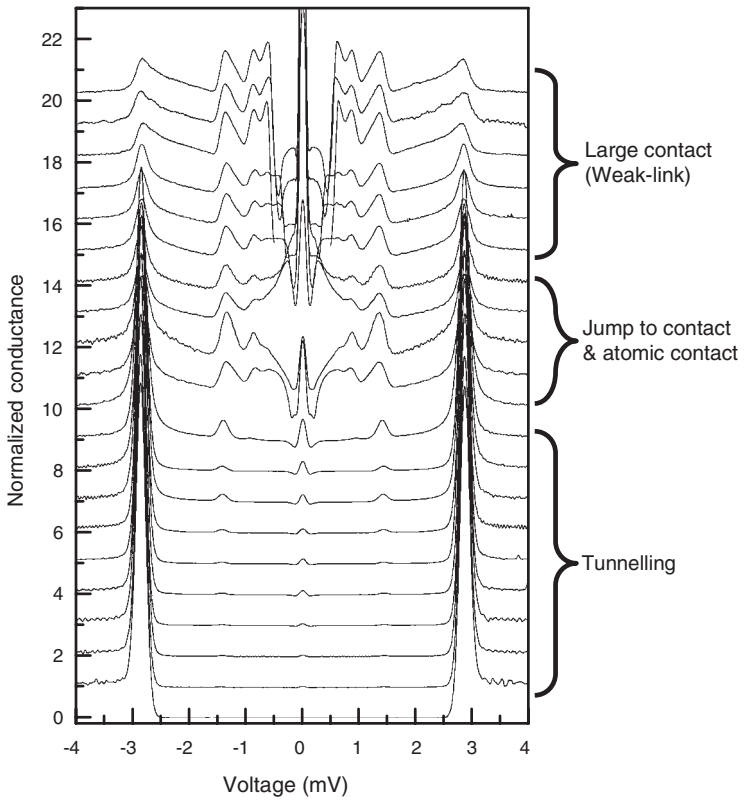

Figure 5. Evolution of the conduction spectra along the different stages of the creation of a Pb nanostructure (nanobridge). For a given nanostructure, it covers resistances from 100 Ω (large point contact) up to 10 MΩ (vacuum tunnelling). Atomic contact takes place for resistances of about 10 kΩ. Measurement performed at 1.8 K. Data from [64].

3.2. Experiment

The method described in section 2 has been used (see [92] and references therein) to create superconducting tips made of lead and aluminium, with transition temperatures of 7.2 and 1.2 K respectively. We will review now the different transport regimes (tunnelling, atomic contact and weak link) accessible through the fabrication and rupture of a superconducting nanobridge. Along this process it is possible to follow in detail the evolution of the I–V characteristics in a wide range of conductance. Figure 5 shows the typical evolution of the conductance spectra, $\mathrm{d}I/\mathrm{d}V$ versus V, as the junction resistance is varied from the vacuum tunnelling regime, 10 MΩ, to a point contact regime with 100 Ω. These STS measurements were made at 1.8 K using a tip and sample made of lead.

3.2.1. Tunnelling regime. Many spectroscopic experiments made with STM on superconductors have shown I–V curves with notable differences with respect to the expected behaviour for a BCS superconductor. It was suggested that the high density of current through the atomic size constrictions could break Cooper pairs, inducing a smearing in the spectroscopic curves [93]. However, it appears that this does not influence the sharpness of the obtained spectra, as emphasized in [47, 92, 94, 95]. Criteria to test the effective resolution of the STM

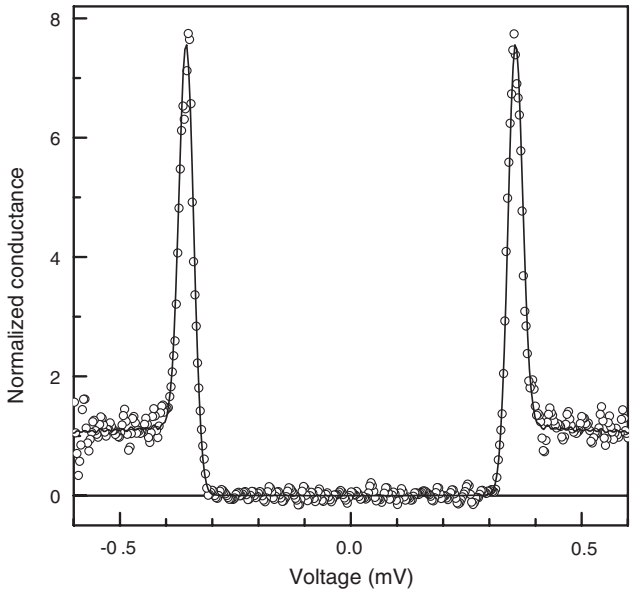

Figure 6. Al–Al tunnelling conductance curve obtained at 70 mK and its corresponding fitting. (Data taken from [92].)

experimental set-up have been discussed in [92, 95], based on measurements on aluminium in ^{3}He/^{4}He dilution refrigerators.

Aluminium is considered in many aspects the archetypical weak-coupling BCS superconductor, with a well defined value of the superconducting gap. Ideal I–V curves in the S–S tunnelling regime at very low temperature present the well known features of zero current up to the gap edge at 2Δ, where there is a jump to non-zero current [65, 96]. This appears in the tunnelling conductance curves ($\mathrm{d}I/\mathrm{d}V$ versus V) as a divergence at energy 2Δ, present at all temperatures, which is the sharpest feature that can be observed in tunnelling spectroscopy measurements in superconductors. Therefore, the measurement of the current in the tunnelling regime is a direct test of the energy resolution of the experimental set-up. This energy resolution can be introduced in the calculus of the curves as a narrow Gaussian distribution, which simulates the noise in the voltage source, and has a halfwidth in energy of σ [92].

Dynes *et al* [97] introduced a phenomenological broadening parameter, Γ, into the BCS density of states to account for the broadening of the gap edges in the spectra of dilute bismuth alloys in lead, as due to finite lifetime effects of the quasiparticles. This lifetime broadening model has been applied routinely to situations in which the main source of smearing or broadening of the spectra is of experimental origin. Figure 6 presents an experimental Al–Al tunnelling conductance curve measured in a dilution refrigerator, and the corresponding fitting [92]. The calculated curve was obtained with the parameters $\Delta = 175\ \mu$eV, $T = 70$ mK (base temperature of the system) and energy halfwidth $\sigma = 15\ \mu$eV. At non-zero temperature the current expected for these junctions at subgap energies is not zero, due to the thermal broadening of the Fermi edge. However, at low temperatures, this current disappears exponentially and it is hardly detectable. Within an experimental resolution in current of 1 pA, the same curve is obtained up to 250 mK.

Tunnelling experiments using superconducting tips obtained from lead nanobridges fabricated with the STM have been reported [43, 92]. Lead is a strong coupling superconductor, and it has been found since early tunnelling experiments [98–100] that its gap value is not

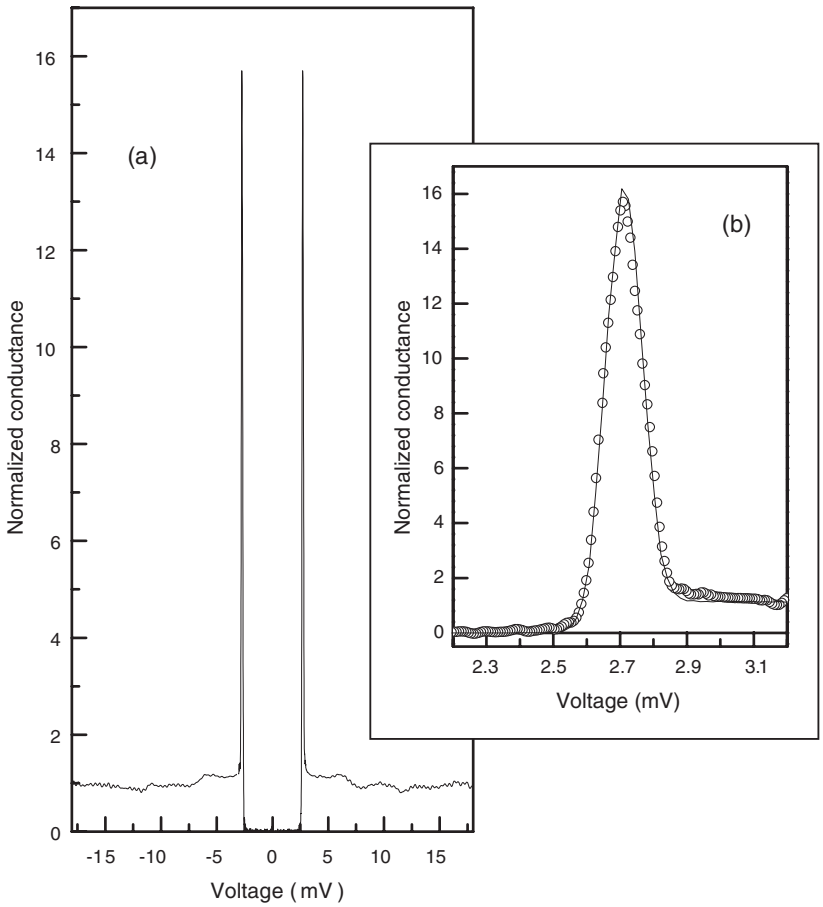

Figure 7. (a) Tunnelling conductance curve obtained in a ^{3}He cryostat at 0.3 K with a tip and sample of Pb ($R_N = 1$ MΩ). (b) Zoom of the gap edge. The theoretical conductance (curve) has been calculated with the parameters described in the text, in order to reproduce the experimental curve (circles). (Data taken from [92].)

constant over the Fermi surface. Recent results give new support to this scenario [101]. The tunnelling curves obtained at 0.3 K (figure 7(a)) present coherence peaks with a finite width, shown in detail in figure 7(b), larger than the one expected considering only the resolution in energy. This additional width is a consequence of the gap distribution in lead. The conductance curves are flat bottomed at a zero value of the conductance inside the gap region, indicating the absence of a relevant finite lifetime source. Therefore, the experimental spectra were simulated by means of a Gaussian distribution of gap values, as well as a similar distribution accounting for the energy resolution of the spectroscopic system. To fit the experimental data for lead, the temperature (0.3 K) and energy resolution ($\sigma = 20$ μeV) were kept fixed, leaving the superconducting gap, Δ, and the halfwidth of the distribution of values of the superconducting gap, δ, as free parameters, obtaining $\Delta = 1.35$ meV and $\delta = 25$ μeV. A detailed discussion of this analysis can be found in [43] and [92].

As lead is a strong-coupling superconductor, the features due to phonon modes are observed in the tunnelling conductance curves (figure 7(a)). According to the well known properties of strong-coupling superconductors [102, 103], a peak in the effective phonon spectrum gives a peak in the voltage derivative of the conductance located at $\Delta_0 + \omega_{L,T}$, with $\omega_{L,T}$ being

the energies corresponding to the phonon modes. No significant difference either in the value of the superconducting gap or in the phonon modes ($\omega_T = 4.4$ meV and $\omega_L = 8.6$ meV) with respect to planar junction experiments is found within the experimental resolution. The progressive fading out of phonon features in the S–S tunnelling conductance curves as both electrodes are approached towards contact was discussed by Rodrigo *et al* [104], being a consequence of the mixing of spectroscopic information from different energies close to the Fermi level as multiple Andreev reflection processes become more important to the total conduction.

Quasiparticle tunnelling is not the only contribution to the total current. It is also possible to observe tunnelling of Cooper pairs, the Josephson effect. As noted in [45, 105–108], the measurement of the Josephson effect in atomic-size and high-resistance vacuum junctions is a true challenge. In a typical tunnelling experiment, with normal-state resistances in the megaohm range, and not very low temperatures, the thermal energy $k_B T$ is higher than the Josephson coupling energy E_J (equation (4)). For Pb junctions with a normal-state resistance of 1 MΩ, both energies are similar at 50 mK. For thermal energies bigger than, but comparable, to the Josephson binding energy, pair tunnelling would be observed, but the pair current will be dissipative, i.e. with the voltage drop proportional to the rate of thermally induced phase slips across the junction [105, 106]. Experiments on ultrasmall Josephson junctions have shown that the Ambegaokar–Baratoff critical current can be reached at low temperature, if the junction is placed in an appropriate controlled electromagnetic environment [109].

By reducing the distance between tip and sample, it is possible to cover a wide range of resistance and temperatures [92, 105, 106, 110], and to get information on different Josephson regimes by changing in a controlled way the ratio between thermal and Josephson binding energies. The increase of the Josephson current as the tunnel resistance is decreased is shown in the inset of figure 8(a). This effect appears as an increasing peak at zero bias in the conductance curves, observed in the lower curves of figure 5, which are normalized and blown up in figure 8(b).

It is important to remark that only the precise determination of the limits in spectroscopic resolution permits us to extract relevant information, such as the gap distribution in lead, from local tunnelling experiments. Recently there have been several reports on new superconducting materials which indicate that a single gap in the Fermi surface is not the most frequent case [92, 95, 111–113]. Multiband superconductivity and gap anisotropy seem to be more ubiquitous than previously thought. These observations enhance the importance of precise local tunnel measurements to shed light on a variety of open problems.

The STM superconducting tip resulting from the rupture of a nanobridge, *in situ* at low temperatures, has been used recently [43, 92] to obtain spectroscopic information and topographic images with atomic resolution on other samples. This was possible by using sample holders like the one described in section 2. Other simultaneous STM/STS experiments using superconducting tips have been reported in the past. A Nb tip, previously cleaned at low temperature by field emission, was used by the authors of [45] to perform STS on a $NbSe_2$ sample, whose surface was imaged with atomic resolution. A different approach is described in [114], where a controlled Pb/Ag proximity bilayer was deposited onto precut Pt/Ir tips to obtain STM superconducting tips suitable for STM/STS experiments. Finally, as early as 1994, a surface of lead was scanned at 4.2 K using a tip of the same element resulting from the rupture of a nanobridge, and spectroscopic measurements at different conductance regimes were performed [115].

3.2.2. Atomic-size contact regime. As the two parts of the nanobridge are approached, the transmission probability through the barrier increases, and MAR leads to SGS at voltages $V \leqslant 2\Delta/e$, and to an excess current at large voltages. The appearance of SGS can be seen

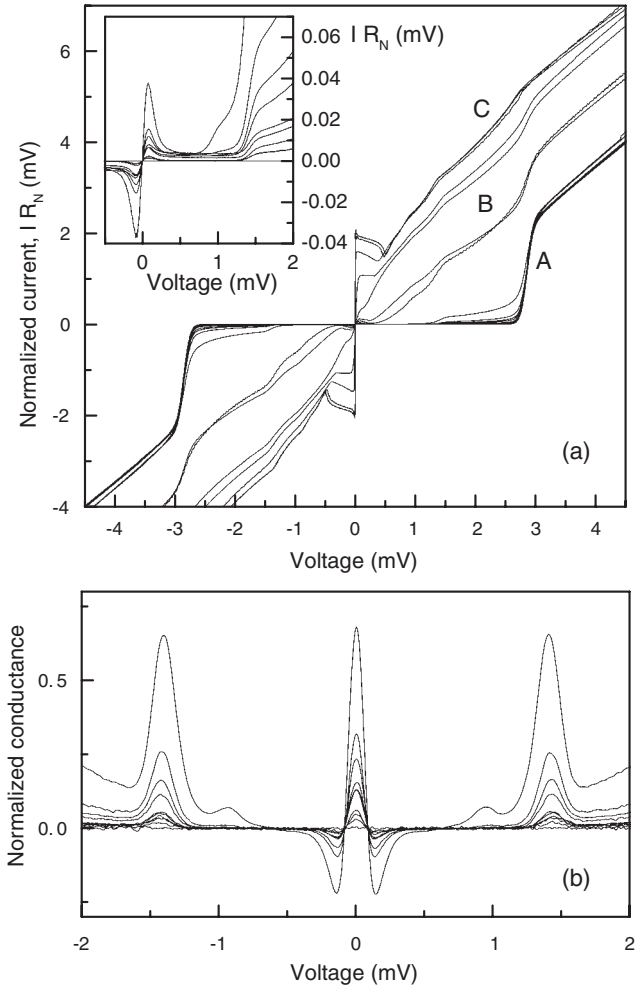

Figure 8. (a) Normalized I–V curves (IR_{N} versus V) corresponding to all the measured range of resistances. The different transport regimes can be identified: tunnelling (A), the transition towards atomic contact between tip and sample (B) and the large-contact regime (C). The SGS features and the excess current develop along the transition from A to C. Inset: blow-up of the region close to zero bias for the curves in tunnelling regime. (b) Normalized conductance curves corresponding to the tunnelling regime. The inset and frame (b) illustrate how the balance between Josephson binding energy and thermal fluctuations affects the observation of Josephson current in the tunnelling regime. (Data from [64]; see also [92].)

in figure 8, both in the current in the inset in (a) and in the normalized conductance in (b). These effects are observed in the curves in figures 5 and 8. Figure 8(a) presents the normalized I–V curves ($I \times R_{\mathrm{N}}$ versus V) corresponding to all the measured range of resistances showing the transition towards contact between tip and sample, and the development of SGS features and the excess current. The SGS features at $V = 2\Delta/ne$ ($n = 1, 2, 3$ and 4), which start to develop in the tunnelling regime, are finally clearly seen in the contact regime (see figure 5). Peaks with high n are enhanced at higher conductance (higher transparency of the barrier) as the probability of multiple Andreev reflections of high order increases.

At present, single-atom contacts can be achieved as a routine procedure. The non-linear I–V curves of these contacts can be fitted to a sum of contributions from the different quantum

channels [59, 60]. The number of conducting channels and their transmission are taken as fitting parameters. The number of channels per atom depends on the chemical element. The individual transmission set changes for different contacts, as shown in figure 16(a). Only three channels are needed to fit these kinds of curves corresponding to Pb contacts [43, 60, 116]. This is taken as an indication that there is a single-atom contact between the nanostructures.

Josephson current has been measured in aluminium atomic point contacts containing a small number of well characterized conduction channels [117]. These contacts were made using microfabricated break junctions. The authors found that the value of the supercurrent is related to the dissipative branch of the I–V characteristics, as in usual macroscopic Josephson junctions, although in the latter the contribution of the different channels cannot be disentangled. This fact strongly supports the idea of the supercurrent being carried by Andreev bound states and shows that the concepts of mesoscopic superconductivity can be applied down to the level of single-atom contacts.

3.2.3. Weak-link regime. When a large point contact is formed between the two parts of the nanobridge, an interesting phenomenology is found in the spectroscopic curves at zero field. As the voltage increases, the system jumps out of the Josephson branch and shows the previously discussed multiple Andreev reflections. Due to the strong current density the temperature rises locally around the contact. The gap decreases and at high voltages the excess current is lost [110, 118]. It vanishes completely when the system locally reaches the critical temperature. This phenomenon appears in the conductance curves as a bump after the SGS, and a recovery of its normal state value when the critical temperature is reached. Heating effects can be controlled *in situ* by changing the form of the neck. Long and narrow bridges will show large overheating effects, whereas short and wide bridges are easily thermalized and much larger voltages have to be applied to observe overheating. Local overheating is also commonly observed in classical point contacts [119–121], although in that case it is not possible to control its magnitude. Figure 9 shows a typical example of conductance curves corresponding to two different nanobridges with the same normal resistance, 500 Ω, equivalent to a minimal cross section of about 20 atoms. The geometry of the bridges can be checked through the evolution of the I–Z curves. Clear heating effects appear in the curve obtained for the long and narrow bridge (curves B) as compared to the situation of a wide bridge (curves A): the SGS peaks move towards lower voltage due to the decrease of the gap value and there is a decrease of conductance, indicative of the loss of the excess current. Finally, the conductance recovers its normal state value as the local temperature rises above T_c. These effects are not present in curve A.

Initial works on lead nanobridges fabricated with a STM [110] reported on the above-mentioned heating effects, as well as on the crossover between the Ambegaokar–Baratoff (tunnelling) and Kulik–Omel'yanchuk (weak-link) limits for the transport of Cooper pairs. Figure 8(a) illustrates the difference in the normalized critical current (i.e. critical voltage) between the tunnelling regime (curves A and inset) and the large-point-contact or weak-link regime (curves C).

4. Superconducting bridges under magnetic fields

4.1. Theoretical models

As mentioned in the introduction, samples of dimensions smaller than or of the order of the London penetration depth are superconducting at magnetic fields well above the bulk critical field. The reduced dimensionality blocks the creation of Meissner screening currents, and

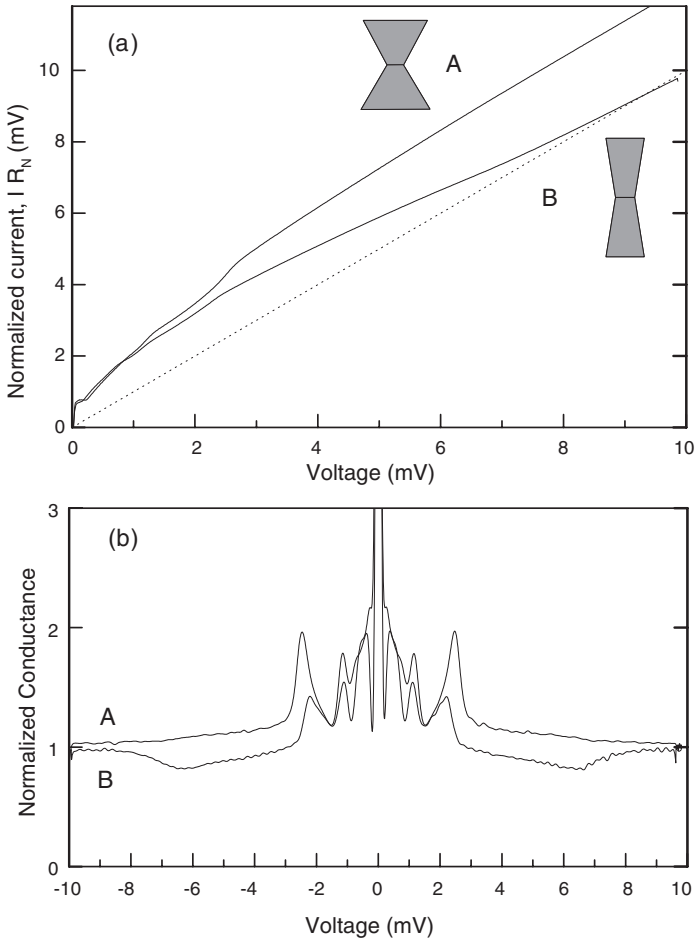

Figure 9. Normalized I–V (a), and conductance (b) curves corresponding to two different nanobridges with the same normal resistance, 500 Ω. Clear heating effects appear for the long and narrow bridge (B). The geometries of both nanobridges are sketched. The dotted curve in (a) indicates the normal state situation. (Data from [64], see also [46].)

the kinetic energy associated with them does not contribute to the total free energy of the superconducting state. The lateral dimensions of typical superconducting nanobridges are easily of the order of, or smaller than, the London penetration depth λ. In the case of Pb, which is the material most intensively studied, the zero-temperature limit of this quantity $\lambda_0 = 32$ nm. Therefore, the superconducting properties of the nanobridge strongly depend on its geometry and on the magnetic field. Several theoretical approaches have been used to describe the experiments. All of them are valid for superconductors in the dirty limit, i.e. with a mean free path ℓ smaller than the superconducting coherence length ξ (in Pb, $\xi_0 = 52$ nm). This assumption is easily justified by the typical lateral dimensions of the nanobridge, which can be taken as a good measure of the order of magnitude of the relevant mean free path ℓ [51, 122]. The reduction of ℓ does not affect the superconducting properties of isotropic, s-wave superconductors [123].

In uniform two-dimensional or one-dimensional structures, such as thin films or wires, the effect of a parallel magnetic field is well described by the pair-breaking theory, reviewed

in [124], and originally developed to account for the effect of magnetic impurities [125]. In contrast to the simple BCS case, in the presence of a pair-breaking mechanism the order parameter and the gap in the spectrum are not equal, and gapless superconductivity is found close to the critical field. As shown below, a more elaborate treatment, the variable-radius pair-breaking model (VRPB), is needed to account for the particular geometry of real nanobridges, which are three-dimensional cone-like objects [116, 126]. The VRPB model uses Usadel's formalism and gives the temperature and magnetic field dependence of the density of states. It reduces to the pair-breaking description [124] when considering a uniform wire. Alternatively, the Ginzburg–Landau (GL) approach has been used to obtain information about the geometrical distribution of the superconducting condensate in the nanobridge, its eventual vorticity and the dependence of the critical current on the field.

4.1.1. Usadel approach; VRPB model. The electronic structure of a superconductor can be described in terms of a 2×2 Green function, which obeys the Gorkov equations. These equations can be simplified when the interesting scale in the problem being considered is much larger than the Fermi wavelength λ_F [127]. In the quasiclassical approximation, the oscillations of the Green function, on a scale of λ_F, are averaged [128]. In the dirty limit the Green function is almost isotropic and an expansion in spherical harmonics keeping only the $L = 0$ term can be made. The Green functions are obtained from Usadel equations [129, 130]. With these assumptions the Green function can be parametrized in terms of two position and energy dependent complex angle variables, $\theta(\vec{r}, E)$ and $\Phi(\vec{r}, E)$ [130–132]:

$$\hat{g}(\vec{r}, E) \equiv \begin{pmatrix} g & f \\ f^\dagger & g \end{pmatrix} \equiv \begin{pmatrix} \cos[\theta(\vec{r}, E)] & \sin[\theta(\vec{r}, E)]\mathrm{e}^{\mathrm{i}\Phi(\vec{r},E)} \\ \sin[\theta(\vec{r}, E)]\mathrm{e}^{-\mathrm{i}\Phi(\vec{r},E)} & \cos[\theta(\vec{r}, E)] \end{pmatrix} \quad (5)$$

g being the ordinary propagator, f the anomalous Green function and $f^\dagger$ its time reverse. Superconductivity is characterized by a non-vanishing f, which gives the probability amplitude for the destruction of a Cooper pair. With this parametrization, the superconducting order parameter $\Delta(\vec{r})$, which has to be determined selfconsistently, and the density of states $N(\vec{r}, E)$ are given by

$$\begin{aligned} \Delta(\vec{r}) &= N_0 V \int_0^{\omega_D} \mathrm{d}E \tanh\left(\frac{E}{K_B T}\right) \mathrm{Im}\left[\sin\theta(\vec{r}, E)\right] \\ N(\vec{r}, E) &= N_0 \,\mathrm{Re}\left[\cos\theta(\vec{r}, E)\right] \end{aligned} \quad (6)$$

with N_0 the normal density of states, and ω_D the Debye frequency. If there is no current $\Phi(\vec{r}, E)$ is a constant equal to the phase of the order parameter and we can drop it in the following.

Let us consider an axially symmetric superconductor in a magnetic field H parallel to its axis. The superconductor is assumed to be thin enough to neglect screening due to superconducting currents, and the vector potential $\vec{A}$ is given by $\vec{A} = \frac{1}{2} H r \vec{e}_\phi$. Usadel's equation can be written as

$$\frac{D}{2}\nabla^2\theta + \left[\mathrm{i}E - \frac{1}{2\tau_{in}}\right]\sin\theta + |\Delta|\cos\theta - \left[\frac{1}{2\tau_{pb}} + 2e^2 D|\vec{A}|^2\right]\cos\theta\sin\theta = 0 \quad (7)$$

where τ_{in} and τ_{pb} are the inelastic and pair-breaking scattering times [124] and $D = \frac{1}{3}\ell v_F$ the diffusion coefficient. When the superconductor is thinner than the coherence length, the radial dependence of the quantities of interest can be neglected, and $\vec{A}^2$ replaced by its average $\langle A^2(z)\rangle = H^2 R^2(z)/12$, where z is the distance to $\vec{r} = 0$ along the superconductor, i.e. parallel to H. The pair-breaking effect of the magnetic field is the given by

$$\Gamma_0^H(z) = e^2 D H^2 R^2(z)/6. \quad (8)$$

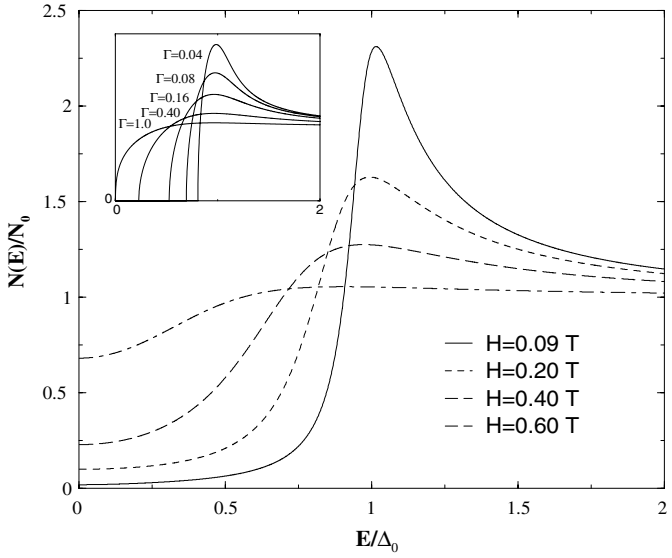

Figure 10. The density of states at the neck calculated using the VRPB model, and corresponding to $L = 850$ Å, $\alpha = 45°$ (see the inset of figure 11), is shown as a function of the magnetic field. The coherence length is reduced to $\xi = 325$ Å to model the changes in ℓ at the nanobridge. In the inset the density of states calculated using a pair-breaking model is represented for different values of Γ. Note the absence of low-energy excitations in a large range of Γ, a point which is not reproduced in the experiments, as discussed further on. (From [116, 126].)

Note that Γ_0^H becomes strongly position dependent and increases, for a fixed field H, with the square of the radius of the sample $R(z)$.

In uniform wires, where R is constant, the pair-breaking term due to the field is also constant in the whole wire and $\nabla\theta = 0$. Neglecting inelastic scattering processes and pair-breaking effects other than those due to the applied field, the following equation is obtained:

$$\frac{E}{|\Delta|} = u\left(1 - \frac{\Gamma}{\sqrt{u^2-1}}\right) \tag{9}$$

where $\Gamma = \Gamma_0^H/|\Delta|$ and the parameter u is defined by $\cos\theta = \frac{u}{\sqrt{u^2-1}}$ and $\sin\theta = \frac{-\mathrm{i}}{\sqrt{u^2-1}}$. In this way, the description for uniform superconductors with pair-breaking effects is recovered [124]. The magnetic field penetrates the superconducting region, inducing pair-breaking effects and reducing the superconducting gap. The density of states, shown in the inset of figure 10, remains gapped up to fields very close to the critical one ($H_{\mathrm{gap}} \sim 0.9 H_{\mathrm{c}}^{\mathrm{wire}}$, with $H_{\mathrm{c}}^{\mathrm{wire}} \sim (\frac{3}{e^2 D})^{1/2}\frac{1}{R}$).

In cone-like nanobridges $R(z)$ and $\Gamma_0^H(z)$ smoothly increase with the distance z with respect to the centre of the structure at a given magnetic field H. The superconducting order parameter will be eventually suppressed at a certain distance, creating an N–S–N structure, in which only the central part of the nanobridge remains in the superconducting state. From equation (7), the magnetic field, temperature and position dependence of the superconducting order parameter and density of states is obtained by introducing an $R(z)$ function which reproduces the geometry of typical nanobridges. R becomes a simple linear function of z if the nanobridge is modelled by two truncated cones each of length L, with an opening angle α, joined by their vertices and attached to bulk electrodes, as shown in the inset of figure 11 [116, 126]. Figure 11 shows the superconducting order parameter as a function of the distance for different applied fields and typical α and L. There is a smooth transition to

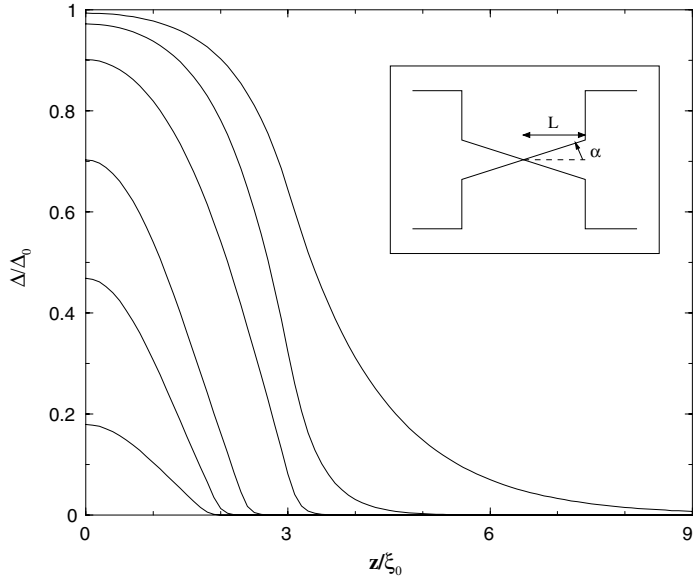

Figure 11. The inset shows the geometry used in the variable-radius description (VRPB). The main figure shows the dependence of the superconducting order parameter, within VRPB, on the distance from the centre of the nanobridge, for different applied fields (from top to bottom, 0.09, 0.2, 0.4 and 0.6 T), using the same geometry as in the previous figure. The neck is joined at the electrodes at $z/\xi = 2.6$. (From [116, 124].)

the normal state as the radius of the nanobridge increases. The magnetic field dependence of the density of states at the centre of the nanobridge, calculated using the same $R(z)$ as in figure 11, is shown in figure 10. A large number of low-energy excitations, induced by the proximity effect from the normal parts of the nanobridge (figure 11), are found in the whole field range. In fact, the superconducting gap is lost already at fields very close to the bulk H_c (0.08 T), which contrasts the case of a uniform wire (inset of figure 10). As shown below, these differences can be addressed experimentally.

4.1.2. Ginzburg–Landau approach. The Ginzburg–Landau (GL) approach [8] has been extensively applied to the study of the distribution of the magnetic field and the superconducting phase in small superconducting systems [16, 17, 133]. A very good account of the geometrical distribution of the order parameter is obtained, although the details of the density of states are more difficult to address. Its applicability is, in principle, restricted to temperatures close to T_c, where it becomes equivalent to Usadel's formalism [134].

The theoretical analysis makes use of the similarities between the Ginzburg–Landau equations for planar superconductors in a magnetic field and the Schrödinger equation for a particle in a field [135]. The predicted magnetic structure is very rich [19, 20], and it has been compared with experiments [18, 136]. Characteristic vortex configurations observed in [18, 136] originate from the competition between the vortex–vortex interaction and the vortex–sample edge interaction [137].

GL equations have been also applied to study the distribution of the superconducting phase in an isolated (non-connected to large electrodes) cone-like geometry [138, 139], which precisely models the nanobridge created in [122] (see figure 12). The 3D equations have been solved, relaxing the assumption of an order parameter constant in the radial direction.

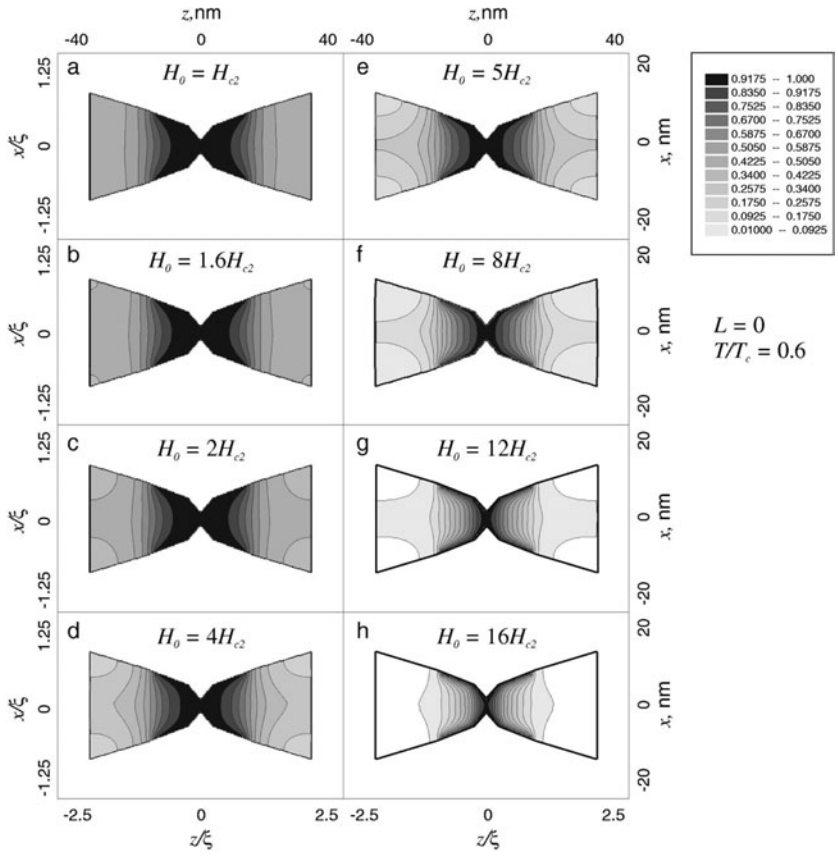

Figure 12. Distribution of the superconducting order parameter in a nanostructure at different magnetic fields (at $T/T_c = 0.6$) (from [138]). Superconductivity survives at the central part of the neck up to fields much higher than the bulk critical one.

These results confirm the applicability of the VRPB model. Already at low magnetic fields, it is found that the parts of the nanobridge with larger radius transit to the resistive state. At the highest magnetic fields, the superconducting phase is concentrated near the neck of the bridge, and very interesting ring-shape areas, indicating states with finite vorticity, appear in a short range of fields and at low temperatures. These calculations have raised the question, not yet addressed in published experiments, of the possible confinement of vortices within the smallest possible superconducting structure. The fundamental properties of these vortex states represent, in our opinion, an interesting field for future studies.

The modification of the critical field of a thin wire by the presence of a current has been also calculated within the GL approach. The critical current, in the absence of the field, is

$$I_c(T) = \frac{H_c(T)R^2c}{3\sqrt{6}\lambda(T)}. \tag{10}$$

In terms of this quantity, the critical field in the presence of a current, and the critical current as function of field can be written as [126]

$$H_c(T, R, I) = H_{wire}(R, T)\sqrt{1 - \left[\frac{I}{I_c(T)}\right]^{2/3}}$$
$$I_c(T, R, H) = I_c(R, T)\left\{1 - \left[\frac{H}{H_{wire}(R, T)}\right]^2\right\}^{3/2} \tag{11}$$

with

$$H_{wire}(T) = \sqrt{32}H_c\frac{\lambda(T)}{R}. \tag{12}$$

An extensive analysis of the functions H_c and I_c can be found in [126]. It is found that a magnetic field above the bulk critical value reduces the critical current. This reduction is more important for wires with larger radius R.

4.2. Experiments

Previously we have discussed the experimental situation at zero magnetic field in the different conduction regimes, tunnelling, atomic-size contact and weak-link regimes. Experiments under magnetic fields confirm the applicability of the VRPB and GL models and show up new effects, associated with the presence of an N–S interface near the centre of the nanobridge.

4.2.1. Tunnelling regime. The tunnelling conductance in the superconducting state has been measured following the rupture of narrow and symmetric nanobridges of Pb [92, 140, 141]. In these tunnel junctions, superconducting correlations have been observed up to magnetic fields as high as 2 T, i.e. at fields 25 times higher than the zero-temperature critical field of bulk samples (0.08 T). In all cases, a large number of low-energy excitations are observed, which can only be explained taking properly into account the geometry of this structure, as in the VRPB model.

I–V curves calculated with the constant pair-breaking model [124] do not reproduce the large current found in the low-voltage part of the measured I–V curves, as shown in the inset of figure 13(a). By contrast, the VRPB model, using parameters consistent with the geometry of typical nanobridges, leads to calculated I–V curves which do indeed follow the experiment, as shown in figure 13(a) and (b) for two different samples. Note that the same geometry is used to fit the whole field range. The large amount of current found in this range is the result of the excitations induced by the proximity effect from the parts of the nanobridge with largest radius, which transit to the normal state at smaller fields than the central part of the nanobridge (figure 11). The destruction of superconducting correlations is a combined effect of the proximity from the perfectly connected normal parts around the superconducting neck, and the pair-breaking effect of the magnetic field. These results show, quite unambiguously, that the magnetic field restricts the volume of the superconducting phase to its minimal size.

The features in the density of states corresponding to the phonon structure (see figure 7) have been followed as a function of the magnetic field in [140], giving the unique possibility to study the pair formation when, gradually, superconductivity is confined to the smallest length scales. In figure 14 the variation of the characteristic phonon modes is shown as a function of the magnetic field. To normalize the position in energy of the phonon features, following previous experiments and calculations for thin films in [142, 143], the phonon frequencies $\omega_{L,T}$ are subtracted from the voltage position of the features corresponding to the transverse and longitudinal phonons $\epsilon_{L,T}$, and divided by twice the zero-field superconducting gap $2\Delta_0$. The data (figure 14) follow well the calculations of [143], intended to explain the experiments in thin films [142]. The confinement of the superconducting correlations to its minimal size

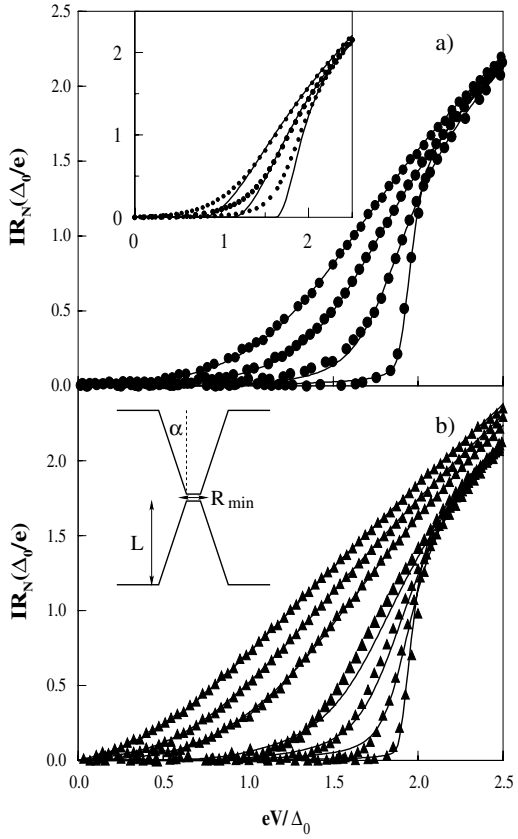

Figure 13. Current (symbols) as a function of bias voltage at $T = 0.4$ K (a), from bottom to top $H = 0, 0.13, 0.18, 0.23$ T, and $T = 1.5$ K (b), from bottom to top $H = 0, 0.17, 0.34, 0.5, 0.84, 1.01, 1.18$ T, for two characteristic nanobridges with the magnetic field applied parallel to the bridge in (a) and perpendicular in (b). Solid curves correspond to the fittings obtained within a variable-radius geometry (VRPB, see inset in (b) and figure 11). The inset in (a) shows calculations (curves) together with experimental curves (points) using a single pair-breaking parameter (inset in figure 10, from bottom to top $\Gamma_0 = 0.04, 0.13, 0.21$). This model does not reproduce the large measured current at low voltages. (From [140].)

by increasing the magnetic field occurs without specially marked changes in the way the Cooper pairs are formed. The perfect connection between the smallest superconducting part of the nanobridge and the large bulk in the normal state is the key element to understand the superconducting state under magnetic fields in these nanostructures.

Somewhat different experiments have been done by transporting one half of the broken nanobridge, i.e. a nanotip (see figure 2), to a flatter region on the Pb sample [92]. In that case, the flat region of the sample is in the normal state, while the tip remains superconducting under field, resulting in characteristic N–S tunnelling curves, which can only be satisfactorily explained within the VRPB model. In figure 15 representative series of data taken as a function of temperature (a) and the corresponding theoretical calculations (b) are shown. Again, these results evidence the strong reduction of the size of the superconducting part under magnetic fields.

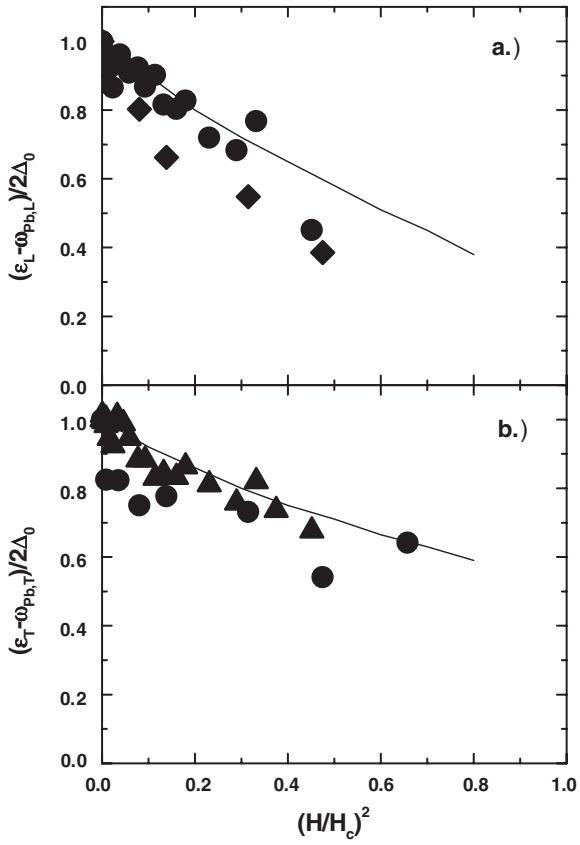

Figure 14. The strong-coupling features corresponding to the longitudinal (a) and transversal (b) phonon modes ($\omega_{L,T}$) are shown as a function of the magnetic field. The data are extracted directly from the position of the corresponding features in the tunnelling density of states ($\epsilon_{L,T}$), and plotted normalized to the superconducting gap at each field. The theory developed by [143] (curves) explains the data. (From [140].)

4.2.2. Atomic-size contact regime. The multiple Andreev reflection pattern has been followed as a function of the magnetic field in many single-atom point contacts made in nanobridges with different geometries [116, 126, 141]. The atomic arrangements around the contacting atom are easily changed without destroying the overall shape of the nanobridge, so that a large series of contacts can be studied at a given magnetic field. The subharmonic gap structure (SGS) is gradually smeared out by the magnetic field.

I–V curves made under magnetic fields in some nanobridges have been reproduced using a uniform pair-breaking parameter Γ and the typical distribution of conduction channels found in Pb (figure 16). However, the magnetic field dependence of Γ was found to be inconsistent with formula (8), making it impossible to give a physical meaning to the values of Γ used within this description [116]. Moreover, subsequent work [126] has found significant discrepancies in situations where the N–S interface moves close to the contact, e.g. at fields close to the complete destruction of superconductivity. The VRPB model, by contrast, gives an adequate fit to the experiment in every case, as shown in a representative example of curves in figure 17. The same geometry, compatible with the one determined experimentally, is used for a given nanobridge in the whole magnetic field range [116].

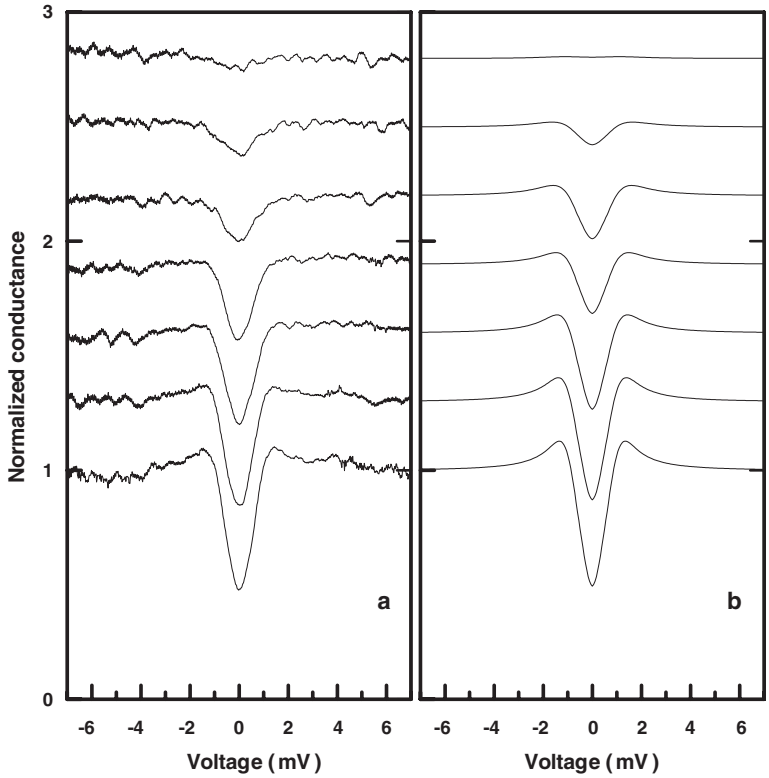

Figure 15. After the creation of the nanostructure, if the tip is transported to a region of the sample which is flat, curves characteristic of N–S junctions are obtained, with the superconducting density of states showing a large number of low-energy excitations (experiment, (a)), explained within the variable-geometry model of [116] (calculated curves in (b)). From bottom to top, $T = 1.0, 1.5, 2.0, 2.5, 3.0, 3.5, 4.0$ K.

A remarkable conclusion of these experiments is that the magnetic field does not change the essential properties of the atomic-size contact, in the sense that the same distribution of conduction channels is needed to fit the experiments. When the field is applied no conduction channel is closed nor does a new channel open [116]. In fact, the flux going through the contact, even at fields of several T, is much too small to produce changes in the electronic transport in the neck or in the orbital structure of the contacting atom.

Other experiments made with the break junction technique in Al also show how atomic-size contact curves are smeared by the application of a magnetic field [144]. In those experiments, one contact was followed as a function of the magnetic field to maintain the distribution of channels constant in the whole field sweep. Their results were interpreted using the pair-breaking model to account for the influence of the magnetic field. However, superconductivity was lost at the bulk critical field of Al (9.9 mT). This technique does not produce nanobridges, so that the region surrounding the contact has the same magnetic response as the bulk, which is in the Meissner state. The magnetic field distribution around the contact should be complex due to demagnetization effects.

The fabrication of a nanobridge around the contact, and the concomitant observation of superconductivity above the bulk critical field, is necessary to get an accurate control over the magnetic response of the system.

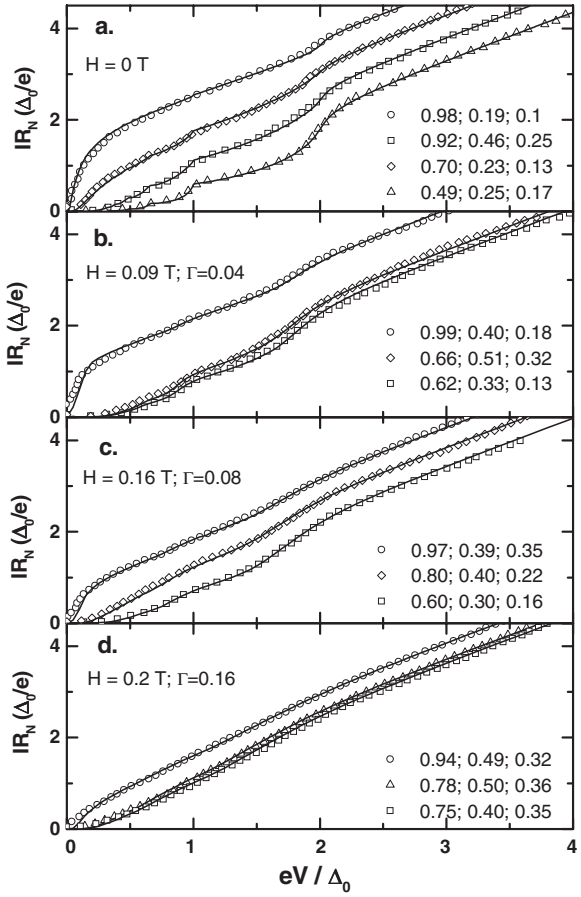

Figure 16. Comparison of theoretical (curves) and experimental (symbols) single-atom contact I–V curves. Theoretical curves correspond to the constant pair-breaking model. Note that the expected field dependence of $\Gamma \propto H^2$ (equation (8)) within this model is not found when trying to reproduce the experiment. The parameters in the lower right corner of each figure are the transmissions through the different channels used to fit the experimental data. Each line of numbers corresponds to one curve, from top to bottom. Γ is the pair-breaking parameter defined in the text.

4.2.3. Weak-link regime. As discussed above (section 3.2.3), cone-like structures which are connected through a large contact of several nanometres in radius show considerable local overheating effects (figure 9). As a consequence, a bump, indicative of the loss of the excess current (formula (3)), appears in the differential conductance. Under magnetic fields, the position of the bump moves to smaller voltages, due to the decrease of the superconducting order parameter.

Interesting situations have been reported in which the conductance shows two bumps whose voltage positions have different magnetic field behaviours. These results have been interpreted as being characteristic of asymmetric nanobridges, in which each half of the cone-like structure has a different opening angle, and therefore also a different power dissipation rate [145]. The half with a smaller opening angle is more easily heated than the half with a larger opening angle. However, the former has a higher critical field than the latter. Correspondingly, while the position of the feature corresponding to the first loss of the excess current (the side with the smaller opening angle becoming normal) remains almost constant, the voltage at

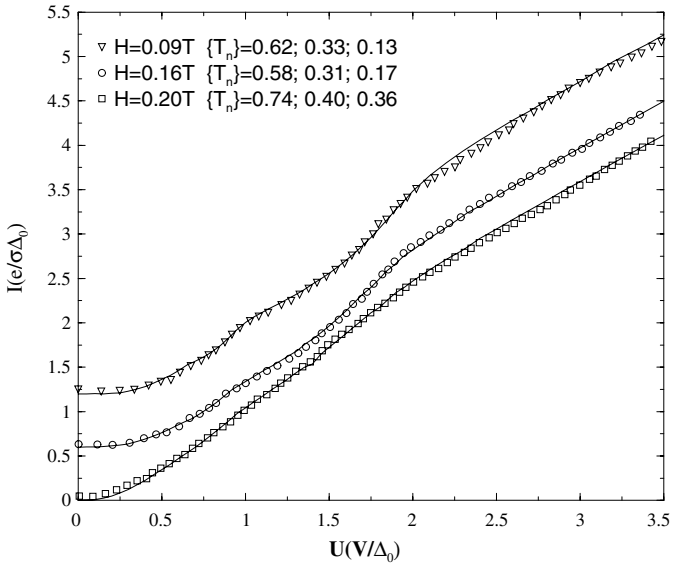

Figure 17. Comparison of several theoretical (curves) and experimental (points) atomic-size contact I–V curves (data are shifted for clarity). Theoretical curves, calculated using the VRPB model, correspond to a geometry with $L = 850$ Å, $\alpha = 45°$ and $\xi = 325$ Å.

which the second loss takes place (the side with larger opening angle) varies strongly with the applied field. These experiments show that it is possible to obtain relevant information about the nanobridge by a careful analysis of the observed I–V curves in the weak-link regime.

On the other hand, in sufficiently long and narrow nanobridges with a symmetric geometry a striking phenomenology has been found with two well defined regimes as a function of the magnetic field [46]. A series of peaks appears in the differential resistance below a magnetic field which corresponds to about half of the field for the complete destruction of superconductivity (0.2 T in figure 18) [46]. These peaks are located at different voltages, but always well above the superconducting gap, and have been associated with the appearance of resistive centres in the nanobridge, in close analogy to the phase slip centres observed in thin wires [91]. At higher fields (above 0.23 T in figure 18), a new regime sets in. The differential resistance steeply increases with the voltage, and abruptly drops to its normal state value when the local critical temperature is reached. This results in a single sharp peak, instead of the smooth structure observed at zero field, which disappears abruptly at the critical temperature, and is always observed when the N–S interface moves close to the central part of the nanobridge, for instance near T_c [46, 145]. Therefore, it has been associated with the establishment of a region within the superconducting nanobridge, where a finite voltage drops. This voltage has been attributed to a non-equilibrium situation created by the conversion of normal current into a supercurrent, as expected near N–S interfaces [146]. Several experiments and theoretical calculations have addressed the observation of such non-equilibrium voltages in thin films, nanolithography structures or nanoscopic wires [91, 146–153]. The nanobridges created with the STM have two remarkable differences with respect to those structures. First, the N–S interface is formed in a natural way within the same material, eliminating possible interface problems, which may appear in evaporated structures. Second, nanobridges created by the STM also have much smaller lateral dimensions enhancing the observed non-equilibrium signals.

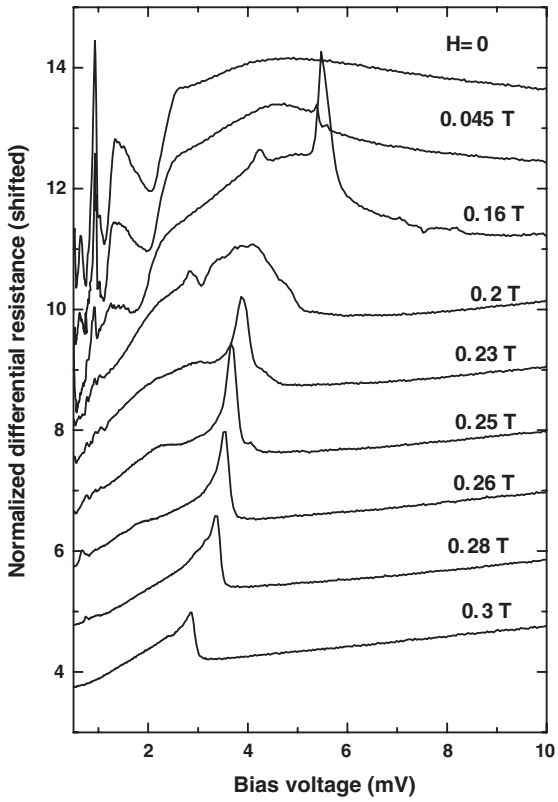

Figure 18. Nanobridges showing heating effects also show a striking behaviour when the magnetic field is applied. Characteristic peaks appear in the differential resistance, indicative of the nucleation of phase slip centres. Above 0.23 T, a single-peak structure appears in the conductance, which has been related to non-equilibrium effects. (From [46].)

Finally, we discuss the Josephson effect, which has been treated in the literature in the large-contact regime with more detail than in the tunnelling and single-atom atomic-size contact regimes. In [122], the critical current has been followed as a function of the size of the contact. The qualitative trend is explained with the calculations using the GL model. In [145], the form of the I–V curve near zero bias is studied. It is shown that at zero field the zero-bias conductance does not diverge, but remains finite between $0.999T_c$ and T_c, an effect typically observed in weak links due to thermally activated phase slip through the barrier [91]. However, this temperature range strongly increases in nanobridges under magnetic fields. In some samples, a finite zero-bias conductance has been observed between $0.3T_c$ and T_c. This is a striking result, and it is unclear if it can solely be explained by the modification of the superconducting order parameter in the VRPB model [145].

5. Advances and future prospects

The nanostructures discussed in this topical review open new interesting fields for basic research and applications. In the following, we will mention some lines in which theoretical and experimental advances could emerge in a near future.

5.1. Theory and fundamental properties

The properties of nanoscopic superconducting bridges in a magnetic field can be reasonably described using adequate extensions of the BCS theory with bulk values for the gap and other relevant parameters. The electron–electron and electron–phonon interactions should be modified near the contact. The structures discussed here are very well suited to analyse these effects. It would be interesting to estimate the influence of the geometry of the contact on the pairing interactions. Some calculations on the properties of these nanobridges under magnetic field [18] have raised the question, not yet addressed in published experiments, of the possible confinement of vortices within the smallest possible superconducting structure. The fundamental properties of these vortex states represent, in our opinion, an interesting field for future studies.

The existence of a close contact between a region of the superconducting phase and a bulky normal phase can allow us to study small differences between the two phases not included in the BCS theory. An interesting effect is a possible charge transfer between the two phases, derived theoretically from different assumptions [154–158].

The electron–electron interactions in mesoscopic devices closely connected to bulk electrodes is a topic of significant theoretical interest [159, 160], as these systems show Coulomb blockade features similar to those found in weakly coupled systems [161, 162]. It will be interesting to know if this enhancement of the repulsive interactions modifies the superconducting properties of the junction at very low temperatures.

The systems studied here, as discussed earlier, allow us to study superconductors where the gap is not constant throughout the Fermi surface. In these materials, elastic scattering by lattice imperfections is a source of pair-breaking processes, playing a similar role to scattering by magnetic impurities in ordinary superconductors. The surface of the sample itself leads to transitions between different bands, or different regions of the Fermi surface [163], and it can change locally the superconducting properties of materials where the gap is not constant, as is probably the case in MgB_2 [164]. This effect has not yet been studied in detail.

5.2. The use of superconducting tips

The capability of the method described in section 2 to prepare and characterize STM tips at low temperatures will open new possibilities. Cleanness and atomic sharpness can be guaranteed and easily restored if needed during operation. One of the applications recently pointed out is the use of well characterized superconducting tips to do scanning Josephson spectroscopy (SJS) [105, 108]. This technique is a very promising way to obtain important information on the nature of the order parameter of several superconducting materials, especially when a non-conventional behaviour opens new challenges [95, 165–168]. As noted in section 4, the knowledge achieved on the behaviour under magnetic fields of those superconducting tips is also important. As has been remarked, the electronic density of states at the tip can be changed by modifying its shape, temperature and external magnetic field. This leads to a series of situations, in which the superconducting condensate is confined to a nanometric size region [145], whose relevance goes beyond the phenomena discussed in this review. In situations where the Zeeman effect is important, superconducting tips under magnetic fields should show a spin split density of states [96], becoming a very sensitive probe of the local spin polarization of the sample. Samples with magnetic inhomogeneities such as vortices or ferromagnetic domains will alternate the density of states of the tip while scanning above them, providing a new nanoprobe within the family of the STM.

5.3. Fluctuations and non-equilibrium effects

During past years, several works have shown that in wires of lateral dimensions even much larger than those of the nanobridges discussed in this review the resistivity does not go to zero when cooling well below T_c [22, 23, 152, 153, 169]. This is explained by the appearance of quantum phase slip centres, i.e. phase slippage induced by quantum tunnelling through the relevant energy barrier, and not by thermal activation. The fundamental question about the way to include the influence of dissipation [170] in those systems has been the subject of recent debate, and the resistance of the wires has been advanced as the actual source of dissipation [22, 23]. The nanobridges that are the subject of this review are perfectly joined to the bulk, and represent an interesting alternative way of confining superconductivity, which seems, *a priori*, to lead to more stable properties at all temperatures. The role of the dissipation should be associated with the proximity to the bulk, instead of the resistance of the structure, and it should be very strong in any case. The large range of temperatures in which a finite zero-bias conductance has been observed under magnetic fields [145] contrasts with the observations at zero field and shows that the confinement of the condensate to the smallest length scales increases the influence of fluctuations. The role of quantum fluctuations in explaining this behaviour of nanobridges remains an interesting question for future work.

5.4. The ultimate nanostructure

In a recent experiment Rubio-Bollinger *et al* [61] have used the STM to study the transport between two proximity induced superconducting electrodes. Nanocontacts were produced between two wires of Pb, in an original experimental arrangement which permitted us to study many different contacts. The wires were arranged as a cross in such a way as to change easily the position where contact is made by using an *in situ* working x–y table. The wires were made of bulk lead covered by a thick layer of lead ($\approx$900 nm), ensuring a clean surface, and subsequently evaporating, *in situ* on top of the Pb layer, a thin layer of gold, $\approx$28 nm in width. In order to minimize inter-diffusion between both elements, the sample was in good thermal contact with a sample holder refrigerated by liquid N_2. Clean single-atom point contacts, and atomic chains of gold between the two wires, could be routinely made with this technique. In the superconducting phase, multiple Andreev reflection processes occur, allowing for a precise determination of the conducting channels across the single-atom point contact. As theoretically expected, in all cases, only a nearly completely opened single channel has been found, not only in single-atom point contacts but also in atomic chains consisting of up to five atoms arranged one after the other. To our knowledge the atomic chain fabricated by these authors using an STM is possibly the smallest weak link between two superconductors ever made. It will be interesting to determine if the chain length affects the coupling between condensates (Josephson effect) or not.

Acknowledgments

We are grateful to our colleagues N Agraït, J P Brison, P C Canfield, G Crabtree, J T Devreese, J Flouquet, V M Fomin, J E Hirsch, A Levanyuk, K Maki, V V Moshchalkov, O Naaman, Y Pogorelov, G Rubio-Bollinger, G Schön and R Villar for their help and stimulating discussions concerning this work at different stages. We acknowledge support from the European Science Foundation programme VORTEX, the MCyT, Spain (grants MAT-2001-1281-C02-0 and MAT2002-0495-C02-01), the Comunidad Autónoma de Madrid, Spain (projects 07N/0039/2002 and 07N/0053/2002), the Swiss National Science Foundation and NCCR MANEP. The Laboratorio de Bajas Temperaturas is associated with the ICMM of the CSIC.

References

[1] Meissner W and Oschenfeld R 1933 *Naturwissenschaften* **21** 787
[2] London F and London H 1935 *Proc. R. Soc.* A **149** 71
[3] London H 1935 *Proc. R. Soc.* A **152** 650
[4] Pontius R B 1937 *Phil. Mag.* **24** 787
[5] Pontius R B 1937 *Nature* **139** 1065
[6] Appleyard E T S, Bristew J A, London H and Misener A D 1939 *Proc. R. Soc.* A **170** 540
[7] Shoenberg D 1940 *Proc. R. Soc.* A **175** 49
[8] Ginzburg V L and Landau L D 1950 *Zh. Eksp. Teor. Fiz.* **20** 1064
[9] Bardeen J, Cooper L N and Schrieffer J R 1957 *Phys. Rev.* **108** 1175
[10] Josephson B D 1962 *Phys. Lett.* **1** 251
[11] Abrikosov A A 1957 *Sov. Phys.—JETP* **5** 1174
[12] Bednorz J G and Muller K A 1985 *Z. Phys.* B **64** 189
[13] Tinkham M 1963 *Phys. Rev.* **129** 2413
[14] Essmann U and Trauble H 1967 *Phys. Lett.* A **24** 426
[15] Dolan G and Silcox J 1973 *Phys. Rev. Lett.* **30** 603
[16] Moshchalkov V V, Gielen L, Strunk C, Jonckheere R, Qiu X, van Haesendonck C and Bruynseraede Y 1995 *Nature* **373** 319
[17] Geim A K, Grigorieva I V, Dubonos S V, Lok J G S, Maan J C, Filippov A E and Peeters F M 1997 *Nature* **390** 259
[18] Misko V R, Fomin V M, Devreese J T and Moshchalkov V V 2003 *Phys. Rev. Lett.* **90** 147003
[19] Schweigert V and Peeters F 1999 *Phys. Rev. Lett.* **83** 2409
[20] Palacios J J 2000 *Phys. Rev. Lett.* **84** 1796
[21] Ralph D C, Black C T and Tinkham M 1997 *Phys. Rev. Lett.* **78** 4087
[22] Lau C N, Markovic N, Bockrath M, Bezryadin A and Tinkham M 2001 *Phys. Rev. Lett.* **87** 217003
[23] Bezryadin A, Lau C N and Tinkham M 2000 *Nature* **404** 971
[24] Kasumov A, Kociak M, Ferrier M, Deblock R, Gueron S, Reulet B, Khodos I, Stephan O and Bouchiat H 2003 *Phys. Rev.* B **68** 214521
[25] Krstic V, Roth S, Burghard M, Weis J and Kern K 2003 *Phys. Rev.* B **68** 205402
[26] Kasumov A, Kociak M, Gueron S, Reulet B, Volkov V, Klinov D and Bouchiat H 2001 *Science* **291** 280
[27] Endres R, Cox D and Singh R 2004 *Rev. Mod. Phys.* **76** 195
[28] Storm A, van Noort J, de Vries S and Dekker C 2001 *Appl. Phys. Lett.* **79** 3881
[29] Hipps K 2001 *Science* **294** 536
[30] Bockrath M, Cobden D, McEuen P, Chopra N, Zettl A, Thess A and Smalley R 1997 *Science* **275** 1922
[31] Binnig G, Rohrer H, Gerber C and Weibel E 1982 *Appl. Phys. Lett.* **40** 178
[32] Binnig G, Quate C F and Gerber C 1986 *Phys. Rev. Lett.* **56** 930
[33] Rubio-Bollinger G, Bahn S R, Agraït N, Jacobsen K W and Vieira S 2001 *Phys. Rev. Lett.* **87** 026101
[34] Martin Y, Williams C C and Wickramasinghe H K 1987 *J. Appl. Phys.* **61** 4723
[35] Oral A, Bending S J and Henini M 1996 *Appl. Phys. Lett.* **69** 1324
[36] Vieira S 1986 *IBM J. Res. Dev.* **30** 553
[37] Gimzewski J K and Möller R 1987 *Phys. Rev.* B **36** 1284
[38] Agraït N, Yeyati A L and van Ruitenbeek J M 2003 *Phys. Rep.* **377** 81
[39] Agraït N, Rodrigo J G, Sirvent C and Vieira S 1993 *Phys. Rev.* B **48** 8499
[40] Pascual J I, Mendez J, Gomez-Herrero J, Baro A M, Garcia N and Binh V T 1993 *Phys. Rev. Lett.* **71** 12
[41] Agraït N, Rodrigo J G, Rubio G, Sirvent C and Vieira S 1994 *Thin Solid Films* **253** 199
[42] Pascual J I, Mendez J, Gomez-Herrero J, Baro A M, Garcia N, Landman U, Luedtke W D, Bogachek E N and Cheng H P 1995 *Science* **267** 5205
[43] Rodrigo J G and Vieira S 2004 *Physica* C **404** 306
[44] Hess H, Robinson R and Waszczak J 1990 *Phys. Rev. Lett.* **64** 2711
[45] Pan S, Hudson E and Davis J 1998 *Appl. Phys. Lett.* **73** 2992
[46] Suderow H and Vieira S 2000 *Phys. Lett.* A **275** 299
[47] Moussy N, Courtois H and Pannetier B 2001 *Rev. Sci. Instrum.* **72** 128
[48] Suderow H, Crespo M, Martínez-Samper P, Rodrigo J G, Rubio-Bollinger G, Vieira S, Luchier N, Brison J P and Canfield P C 2002 *Physica* C **369** 106
[49] Martínez-Samper P, Rodrigo J G, Agraït N, Grande R and Vieira S 2000 *Physica* C **332** 450
[50] Agraït N, Rubio G and Vieira S 1995 *Phys. Rev. Lett.* **74** 3995
[51] Untiedt C, Rubio G, Vieira S and Agraït N 1997 *Phys. Rev.* B **56** 2154

[52] Rodrigo J G, García-Martín A, Sáenz J J and Vieira S 2002 *Phys. Rev. Lett.* **88** 24680
[53] Landman U, Luedtke W D, Burnham N A and Colton R J 1990 *Science* **248** 454
[54] Stafford C A, Baeriswyl D and Burki J 1997 *Phys. Rev. Lett.* **79** 283
[55] Rubio G, Agraït N and Vieira S 1996 *Phys. Rev. Lett.* **76** 2302
[56] Yanson A, Rubio-Bollinger G, van den Brom H, Agraït N and van Ruitenbeek J 1998 *Nature* **395** 783
[57] Landauer 1957 *IBM J. Res. Dev.* **1** 223
[58] Wharam D, Thornton T, Newbury R, Pepper M, Ahmed H, Frost J, Hasko D, Peacock D, Ritchie D and Jones G 1988 *J. Phys. C: Solid State Phys.* **21** L209
[59] Scheer E, Joyez P, Esteve D, Urbina C and Devoret M H 1997 *Phys. Rev. Lett.* **78** 3535
[60] Scheer E, Agraït N, Cuevas J, Levy-Leyati A, Ludolph B, Martín-Rodero A, Rubio-Bollinger G, van Ruitenbeek J and Urbina C 1998 *Nature* **394** 154
[61] Rubio-Bollinger G, de las Heras C, Bascones E, Agraït N, Guinea F and Vieira S 2003 *Phys. Rev.* B **67** 121407
[62] Sharvin Y 1965 *Sov. Phys.—JETP* **21** 655656
[63] Gai Z, Li X, Gao B, Zhao R G, Yang W S and Frenken J W M 1998 *Phys. Rev.* B **58** 2185
[64] Rodrigo J G, Suderow H and Vieira S 2004 unpublished, these data represent the current state of the art of STS on lead nanostructures at the low temperature laboratory, in the Universidad Autonoma de Madrid
[65] Wolf E 1989 *Principles of Electron Tunneling Spectroscopy* (Oxford: Oxford University Press)
[66] Andreev A F 1964 *Sov. Phys.—JETP* **19** 1228
[67] Artemenko S N, Volkov A F and Zaitsev A V 1978 *JETP Lett.* **28** 589
[68] Artemenko S N, Volkov A F and Zaitsev A V 1979 *Sov. Phys.—JETP* **49** 924
[69] Artemenko S N, Volkov A F and Zaitsev A V 1979 *Solid State Commun.* **30** 771
[70] Zaitsev A V 1980 *Sov. Phys.—JETP* **51** 111
[71] deGennes P G 1989 *Superconductivity of Metals and Alloys* (New York: Addison-Wesley)
[72] Blonder G E, Tinkham M and Klapwijk T M 1982 *Phys. Rev.* B **25** 4515
[73] Octavio M, Tinkham M, Blonder G E and Klapwijk T M 1983 *Phys. Rev.* B **27** 6739
[74] Averin D and Bardas A 1995 *Phys. Rev. Lett.* **75** 1831
[75] Cuevas J C, Martín-Rodero A and Levy-Yeyati A 1996 *Phys. Rev.* B **54** 7366
[76] Octavio M, Skocpol W and Tinkham M 1978 *Phys. Rev.* B **17** 159
[77] Bascones E and Guinea F 2002 *Phys. Rev.* B **65** 174505
[78] Bardas A and Averin D 1997 *Phys. Rev. Lett.* **79** 3482
[79] Josephson B D 1965 *Adv. Phys.* **14** 419
[80] Barone A and Paterno G 1982 *Physics and Applications of the Josephson Effect* (New York: Wiley)
[81] Ambegaokar V and Baratoff A 1963 *Phys. Rev. Lett.* **10** 486
[82] Likharev K K 1979 *Rev. Mod. Phys.* **51** 101
[83] Kulik I and Omelyanchuk A 1975 *JETP Lett.* **21** 96
[84] Beenakker C and van Houten H 1991 *Phys. Rev. Lett.* **66** 3056
[85] Beenakker C 1991 *Phys. Rev. Lett.* **67** 3836
[86] Ivanchenko M and Zilberman L A 1969 *Sov. Phys.—JETP* **28** 1272
[87] Harada Y, Takayanagi H and Odintsov A A 1996 *Phys. Rev.* B **54** 6608
[88] Martinis J M and Kautz R L 1989 *Phys. Rev. Lett.* **63** 1507
[89] Ingold G L, Grabert H and Eberhardt U 1994 *Phys. Rev.* B **50** 395
[90] Vion D, Gotz M, Joyez P, Esteve D and Devoret M H 1996 *Phys. Rev. Lett.* **77** 3435
[91] Tinkham M 1996 *Introduction to Superconductivity* (Singapore: McGraw International)
[92] Rodrigo J G, Suderow H and Vieira S 2004 *Eur. Phys. J.* B submitted
[93] Renner C, Kent A D, Niedermann P, Fischer O and Levy F 1991 *Phys. Rev. Lett.* **67** 1650
[94] Suderow H, Martínez-Samper P, Luchier N, Brison J P, Vieira S and Canfield P C 2001 *Phys. Rev.* B **64** 02503
[95] Suderow H, Vieira S, Strand J D, Budko S and Canfield P C 2004 *Phys. Rev.* B **69** 060504
[96] Mersevey R and Tedrow P 1994 *Phys. Rep.* **238** 173
[97] Dynes R C, Narayanamurti V and Garno J P 1978 *Phys. Rev. Lett.* **41** 1509
[98] Blackford B L and March R H 1969 *Phys. Rev.* **186** 397
[99] Lykken G I, Geiger A L, Dy K S and Mitchell E N 1971 *Phys. Rev.* B **4** 1523
[100] Tomlinson P G and Carbotte J P 1976 *Phys. Rev.* B **13** 4738
[101] Short J and Wolfe J 2000 *Phys. Rev. Lett.* **85** 5198
[102] Eliashberg G 1960 *Zh. Eksp. Teor. Fiz.* **38** 966
[103] McMillan W L and Rowell J M 1965 *Phys. Rev. Lett.* **14** 108
[104] Rodrigo J G, Agraït N, Sirvent C and Vieira S 1994 *Phys. Rev.* B **50** 7177
[105] Naaman O, Teizer W and Dynes R 2001 *Phys. Rev. Lett.* **87** 97004
[106] Naaman O and Dynes R 2004 *Solid State Commun.* **129** 299

[107] Naaman O, Dynes R C and Bucher E 2003 *Int. J. Mod. Phys.* B **17** 3569
[108] Smakov J, Martin I and Balatsky A 2001 *Phys. Rev.* B **64** 212506
[109] Steinbach A, Joyez P, Cottet A, Esteve D, Devoret M H, Huber M E and Martinis J M 2001 *Phys. Rev. Lett.* **87** 137003
[110] Rodrigo J G, Agraït N and Vieira S 1994 *Phys. Rev.* B **50** 12788
[111] Rubio-Bollinger G, Suderow H and Vieira S 2001 *Phys. Rev. Lett.* **86** 5582
[112] Boaknin E *et al* 2003 *Phys. Rev. Lett.* **90** 117003
[113] Yokoya T, Kiss T, Chainani A, Shin S, Nohara M and Takagi H 2001 *Science* **294** 2518
[114] Naaman O, Teizer W and Dynes R 2001 *Rev. Sci. Instrum.* **72** 1688
[115] Rodrigo J G, Agraït N and Vieira S 1994 *Phys. Rev.* B **50** 374
[116] Suderow H, Bascones E, Belzig W, Guinea F and Vieira S 2000 *Europhys. Lett.* **50** 749
[117] Goffman M F, Cron R, Yeyati A L, Joyez P, Devoret M H, Esteve D and Urbina C 2000 *Phys. Rev. Lett.* **85** 170
[118] Flensberg K and Hansen J B 1989 *Phys. Rev.* B **40** 8693
[119] Duif A M, Jansen A G M and Wyder P 1987 *J. Magn. Magn. Mater.* **63/64** 664
[120] Duif A M, Jansen A G M and Wyder P 1989 *J. Phys.: Condens. Matter* **1** 3157
[121] Jansen A G M, van Gelder A and Wyder P 1980 *J. Phys. C: Solid State Phys.* **13** 6073
[122] Poza M, Bascones E, Rodrigo J G, Agraït N, Vieira S and Guinea F 1998 *Phys. Rev.* B **58** 11173
[123] Anderson P W 1959 *J. Phys. Chem. Solids* **11** 26
[124] Maki K 1966 *Superconductivity* (New York: Dekker) p 1035
[125] Abrikosov A and Gorkov L 1961 *Sov. Phys.—JETP* **12** 1243
[126] Bascones E 2000 *PhD Thesis* Universidad Autónoma de Madrid
[127] Eilenberger G 1968 *Z. Phys.* **214** 195
[128] Rammer J and Smith H 1986 *Rev. Mod. Phys.* **58** 323
[129] Usadel K D 1970 *Phys. Rev. Lett.* **25** 507
[130] Belzig W, Wilhelm F, Bruder C, Schön G and Zaikin A 1999 *Superlatt. Microstruct.* **25** 1251
[131] Golubov A and Kupriyanov M 1988 *J. Low Temp. Phys.* **70** 83
[132] Stoof T and Nazarov Y 1996 *Phys. Rev.* B **53** 14496
[133] Geim A, Dubonos S V, Lok J G S, Henin M and Maan J 1998 *Nature* **396** 6707
[134] Maki K 1964 *Prog. Theor. Phys.* **32** 29
[135] Palacios J J 1998 *Phys. Rev.* B **58** R5948
[136] Geim A K, Dubonos S V, Palacios J J, Grigorieva I V, Henini M and Schermer J J 2000 *Phys. Rev. Lett.* **85** 1528
[137] Baelus B J and Peeters F M 2002 *Phys. Rev.* B **65** 104515
[138] Misko V R, Fomin V M and Devreese J T 2001 *Phys. Rev.* B **64** 014517
[139] Misko V, Fomin V and Devreese J 2002 *Physica* C **369** 356
[140] Suderow H, Bascones E, Izquierdo A, Guinea F and Vieira S 2002 *Phys. Rev.* B **65** 100519
[141] Suderow H, Izquierdo A and Vieira S 2000 *Physica* C **332** 327
[142] Rasing T, Salemink H W M, Wyder P and Strassler S 1981 *Phys. Rev.* B **23** 4470
[143] Daams J, Zarate H and Carbotte J 1984 *Phys. Rev.* B **30** 2577
[144] Scheer E, Cuevas J C, Yeyati A L, Martín-Rodero A, Joyez P, Devoret M, Esteve D and Urbina C 2000 *Physica* B **280** 425
[145] Rodrigo J G, Suderow H and Vieira S 2003 *Phys. Status Solidi* b **237** 386
[146] Schmid A and Schön G 1979 *Phys. Rev. Lett.* **43** 793
[147] Clarke J, Eckern U, Schmid A, Schön G and Tinkham M 1979 *Phys. Rev.* B **20** 3933
[148] Schmid A and Schön G 1980 *Phys. Rev.* B **21** 5076
[149] Baratoff A 1982 *Phys. Rev. Lett.* **48** 434
[150] Escudero R and Smith H J T 1984 *Phys. Rev.* B **30** 2527
[151] Moshchalkov V V, Gielen L, Neuttiens G, van Haesendonck C and Bruynseraede Y 1994 *Phys. Rev.* B **49** 15412
See also Landau I L and Rinderer L 1997 *Phys. Rev.* B **56** 6348 (Comment)
Moshchalkov V V, Gielen L, Neuttiens G, van Haesendonck C and Bruynseraede Y 1997 *Phys. Rev.* B **56** 6352 (Reply)
[152] Boogaard G R, Verbruggen A H, Belzig W and Klapwijk T M 2004 *Preprint* cond-mat/0401364
[153] Michotte S, Mátéfi-Tempfli S, Piraux L, Vodolazov D Y and Peeters F M 2004 *Phys. Rev.* B **69** 094512
[154] Khomskii D I and Kusmartsev F V 1992 *Phys. Rev.* B **46** 14245
[155] Khomskii D and Freimuth A 1995 *Phys. Rev. Lett.* **75** 1384
[156] Lipavský P, Morawetz K, Kolácek J, Mares J J, Brandt E H and Schreiber M 2004 *Phys. Rev.* B **69** 024524

[157] Hirsch J E 2004 *Phys. Rev. Lett.* **92** 016402
[158] Hirsch J E 2004 *Preprint* cond-mat/0312619
[159] Nazarov Y V 1999 *Phys. Rev. Lett.* **82** 1245
[160] Golubev D S and Zaikin A D 2001 *Phys. Rev. Lett.* **86** 4887
[161] Guinea F and Schön G 1987 *J. Low Temp. Phys.* **69** 219
[162] Grabert H and Devoret M H (ed) 1992 *Single Electron Tunneling* (New York: Plenum)
[163] Bascones E and Guinea F 2001 *Phys. Rev.* B **64** 214508
[164] Martínez-Samper P, Rodrigo J G, Rubio-Bollinger G, Suderow H, Vieira S, Lee S and Tajima S 2003 *Physica* C **385** 233
[165] Aliev F G, Gomez-Sal J C, Suderow H and Villar R (ed) 2000 *Some Modern Aspects of the Physics of Strongly Correlated Electron Systems* (Universidad Autonoma de Madrid) see http://www.uam.es/inc/summerschool99/
[166] Flouquet J 2004 *Prog. Low Temp. Phys.* at press
[167] Joynt R and Taillefer L 2002 *Rev. Mod. Phys.* **74** 235
[168] McElroy K, Simmonds R W, Hoffman J E, Lee D-H, Orenstein J, Eisaki H, Uchida S and Davis J C 2003 *Nature* **422** 592
[169] Vodolazov D Y, Peeters F M, Piraux L, Mátéfi-Tempfli S and Michotte S 2003 *Phys. Rev. Lett.* **91** 157001
[170] Schmid A 1983 *Phys. Rev.* B **51** 1506